Landslide Susceptibility Zonation of Idukki District Using GIS in the Aftermath of 2018 Kerala Floods and Landslides: a Comparison of AHP and Frequency Ratio Methods

Anjana V. Thomas[1] · Sunil Saha[2] · Jean Homian Danumah[3] · S. Raveendran[4] · Megha K. Prasad[5] · R. S. Ajin[4] · Sekhar L. Kuriakose[4]

Abstract

This study aims to demarcate landslide susceptible zones using methods of analytical hierarchy process (AHP) and frequency ratio (FR) to find the most influencing factors and to compare their prediction capability. Ten causative factors (slope angle, elevation, lithology, land use/land cover types, normalized difference moisture index, road buffer, normalized difference built-up index, water ratio index, stream power index, and soil) are used in the study. The area of the landslide susceptibility was grouped into five classes. According to the landslide susceptibility maps prepared using the AHP and FR methods, 11.14% and 6.57% of the area are very highly susceptible to landslides. Finally, the receiver operating characteristic (ROC) curves for the landslide susceptibility maps prepared using both AHP and FR methods were plotted, and the area under the ROC curve (AUC) values were estimated to validate the results. AUC values of 0.69 and 0.81 were estimated for the landslide susceptible zone maps prepared using AHP and FR, respectively. From the AUC values, it is confirmed that the FR method is more effective in predicting the landslide susceptible zones in Idukki district. The landslide susceptibility maps are helpful for land use planners and policy makers in adopting suitable mitigation measures to minimize the impacts of landslides and thereby reduce loss of life and property.

Keywords Analytical hierarchy process · Frequency ratio · GIS · Landslides · Western Ghats

Introduction

A landslide is the downslope movement of debris, rock, or earth material under the influence of gravity (Cruden 1991). Landslides are the most common geohazards occurring in the hilly and mountainous regions and occur when the slope becomes unstable (Chawla et al. 2018). A landslide disaster is a result of intrinsic factors and external (or triggering) factors (Raghuvanshi et al. 2015; Hamza and Raghuvanshi 2017). The intrinsic factors define the favorable or unfavorable stability conditions within the slope (Raghuvanshi et al. 2014). The most common intrinsic factors are slope geometry, slope material, land use and land cover, ground water, and structural discontinuities (Anbalagan 1992). The triggering factors include seismicity (Aimaiti et al. 2019; Nakamura et al. 2014; Sassa et al. 1996), rainfall (Cardinali et al. 2006; Lee et al. 2014; Senthilkumar et al. 2018), and the activities of humans. Excavation of a slope or its toe, loading of the slope or its crest, mining, deforestation, artificial vibration, irrigation, and water leakage from utilities are all examples of human-induced activities (United States Geological Survey 2004).

Landslide disasters lead to thousands of fatalities and cost billions of dollars in property damage worldwide annually (Hong et al. 2007). Landslides play a crucial role

✉ R. S. Ajin
  ajinares@ieee.org; ajinares@gmail.com

1 Department of Geology, University College, Thiruvananthapuram, Kerala, India

2 Department of Geography, University of Gour Banga, Malda, West Bengal, India

3 Centre Universitaire de Recherche Et d'Application en Télédétection (CURAT), Université Félix Houphouët-Boigny, Abidjan, Côte d'Ivoire

4 Kerala State Emergency Operations Centre (KSEOC), Kerala State Disaster Management Authority (KSDMA), Thiruvananthapuram, Kerala, India

5 Department of Remote Sensing, Bharathidasan University, Tiruchirappalli, Tamil Nadu, India

in landscape evolution (Guzzetti et al. 2012). It may also lead to water pollution that destroys fish habitat; alters soil texture, porosity, and density; and destroys farmland and forest cover (Geertsema et al. 2009). In India, about 12.6% of the land area is prone to landslides (Geological Survey of India: https://www.gsi.gov.in). The most landslide-prone areas in India are the Himalayan region (Sarkar et al. 1995; Kaur et al. 2017) and the Western Ghats and Nilgiri range (Kaur et al. 2017). Therefore, there is a need for mapping the landslide susceptible zones so that appropriate mitigation measures for effective disaster management can be implemented.

GIS techniques can be effectively used to delineate landslide susceptible zones. Various methods adopted for delineating landslide susceptible zones include neuro-fuzzy (Pradhan et al. 2010; Oh and Pradhan 2011), artificial neural networks (Lee 2007; Shahri et al. 2019), index of entropy (Pourghasemi et al. 2012a; Jaafari et al. 2014), decision tree models (Zhang et al. 2017; Park et al. 2018), fuzzy logic (Rostami et al. 2016; Aghda et al. 2018), weights of evidence (Kayastha et al. 2012; Elmoulat and Ait Brahim 2018), support vector machine (Pourghasemi et al. 2013; Kumar et al. 2017), and logistic regression (Kouhpeima et al. 2017; Hemasinghe et al. 2018).

The analytical hierarchy process (AHP) is a multi-criteria decision-making approach that allows the user to arrive at a preference scale drawn from a set of alternatives (Semlali et al. 2019). The AHP method enables opinions to be quantified and converted into a consistent decision model, thereby helping solve complex problems (Cancela et al. 2015). The AHP techniques have been effectively used to demarcate the landslide susceptible zones (El Jazouli et al. 2019; Semlali et al. 2019; Dahoua et al. 2018; Sharma and Mahajan 2018; Achour et al. 2017; Chen et al. 2016; Kumar and Anbalagan 2016; Myronidis et al. 2016; Wu et al. 2016; Althuwaynee et al. 2014).

The frequency ratio (FR) method has also been effectively used in demarcating landslide susceptible zones (Oh et al. 2017; Khan et al. 2019; Silalahi et al. 2019; Shano et al. 2021). The FR method is a simple method utilized to determine the correlation between landslide locations and each causative factor (Rasyid et al. 2016).

The objectives of this study are to prepare the landslide susceptible zone maps of Idukki district in Kerala using the AHP and the FR methods, to analyze the influence of landslide causative factors, and to compare the prediction capability of both AHP and FR methods. To prepare the susceptible zone maps, ten causative factors are selected, namely slope angle, elevation, lithology, land use/land cover types, normalized difference moisture index (NDMI), road buffer, normalized difference built-up index (NDBI), water ratio index (WRI), stream power index (SPI), and soil.

Materials and Methods

Study Area

Idukki is the second largest district in Kerala and is situated in the southern Western Ghats (Abraham et al. 2019). The district lies between longitudes of 76° 35′ 0″ E and 77° 25′ 0″ E and latitudes of 9° 15′ 0″ N and 10° 25′ 0″ N and spans an area around 4358 km². This district is bordered by the Tamilnadu state in the North and East, Ernakulam and Kottayam districts in the West, and Pathanamthitta district and Tamilnadu state in the South. The major rivers flowing through this district are Periyar, Thodupuzhayar, Muthirappuzhayar, and Thalayar. The district's 14 mountain peaks exceed a height of 2000 m (Ramachandran and Reddy 2017). Anamudi, the highest peak in the Western Ghats, and the Idukki Dam, one of the highest arch dams in Asia, are in Idukki district (Abraham et al. 2021). The Western Ghats region of India is also prone to landslides and was severely affected by landslides during the 2018 southwest monsoon (Kanungo et al. 2020). A total of 47 landslide deaths were reported, and more than 1000 landslides have occurred in Idukki district during the 2018 southwest monsoon. The catastrophic Pettimudi landslide which resulted in the death of 66 residents is the major landslide reported (in number of deaths) in the Idukki district and in the state (Achu et al. 2021). The exact location of the study area is shown in Fig. 1.

Data used

The study area falls over the Survey of India topographic maps numbered 58 B/16, 58 C/9, 58 C/13, 58 C/14, 58 C/15, 58 F/3, 58 F/4, 58 F/7, 58 F/8, 58 G/1, 58 G/2, 58 G/3, 58 G/5, 58 G/6, and 58 G/7 at 1:50,000 scale. The data used for this modelling includes Survey of India (SoI) topographic maps, Kerala State Land Use Board (KSLUB) soil data, Geological Survey of India (GSI) geological map of Kerala, Landsat 8 OLI (Operational land imager) satellite images, SRTM (Shuttle radar topography mission) DEM (Digital elevation model), and Google Earth Pro data. ERDAS Imagine 8.4 and ArcGIS 10.8 were used to create the thematic layers of the selected factors. The thematic layers of slope angle, elevation, NDMI, NDBI, WRI, and SPI were then classified using the ArcGIS natural breaks classification method. After assigning weights calculated by AHP and FR techniques, the thematic layers were then integrated with the map algebra tool of ArcGIS to derive the landslide susceptible zones. The prepared susceptible zone maps were validated using the landslide incidence data collected from the Bhukosh portal (https://bhukosh.gsi.gov.in/Bhukosh/Public) of GSI. The RStudio
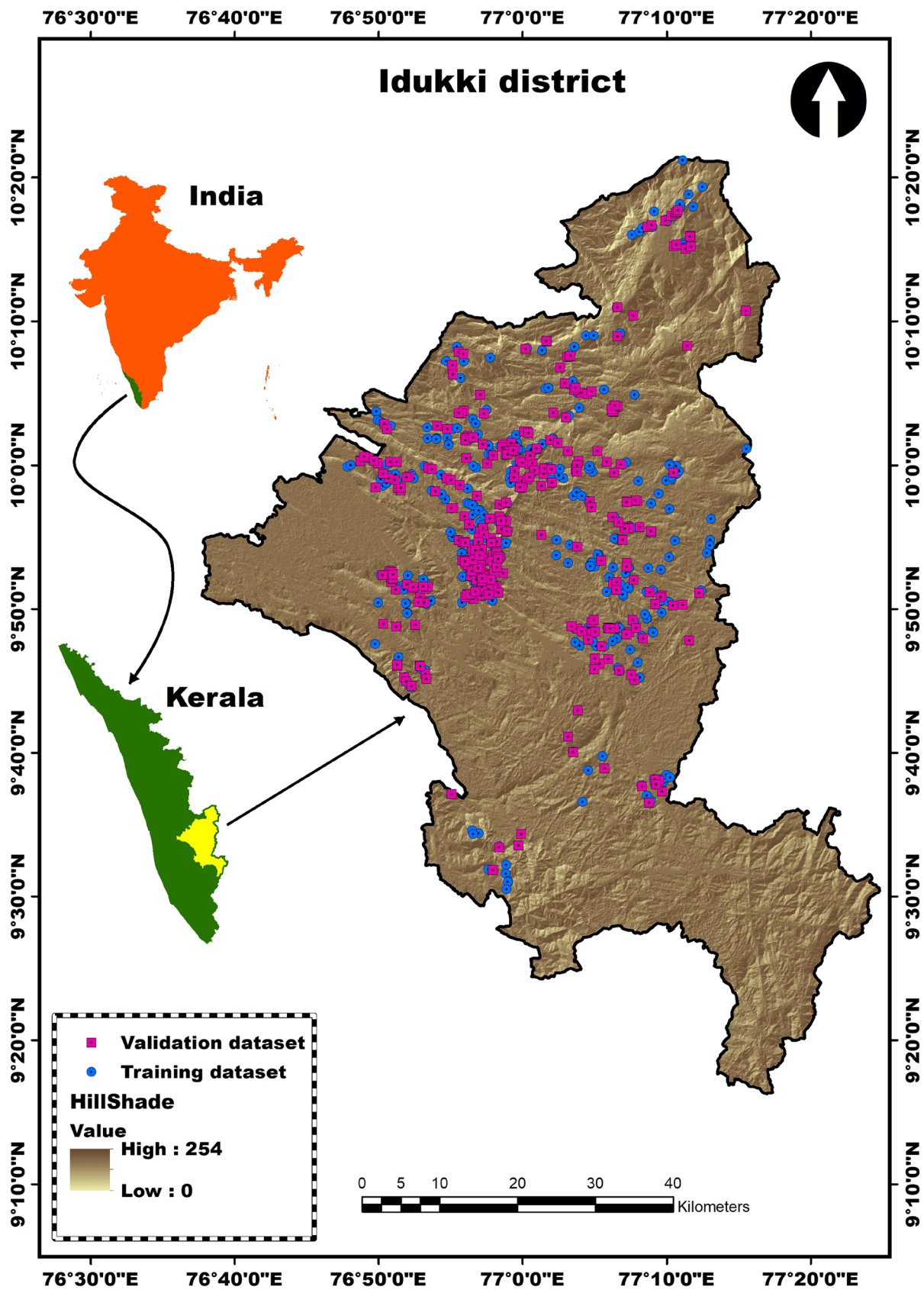
Fig. 1 Idukki district: the study area

software package was used to plot the ROC curves and to estimate the AUC values for the susceptible zone maps prepared using the AHP and the FR models. The flowchart of landslide modelling is shown in Fig. 2.

Causative Factors

Slope angle In general, shear stress in soil generally increases with the angle of the slope (Lee et al. 2004). The shear stress results in the downslope movement of earth materials. Therefore, the chance of landslides is greater in areas with higher slope angles. The slope was generated from the DEM using ArcGIS spatial analyst (surface analysis) tools. The slope of the Idukki district is categorized into five classes: 0–8.90°, 8.90–16.89°, 16.89–25.18°, 25.18–35.93°, and 35.93–78.32° (Fig. 3).

Elevation Landslides generally occur at intermediate elevations, because slopes of that terrain usually contain thin layers of colluviums that are susceptible to landslides (Dai

and Lee 2002). A DEM has been used to derive the elevation of the district using ArcGIS spatial analyst tools. The study area's elevation is divided into five classes: 13–457 m, 457–904 m, 904–1306 m, 1306–1802 m, and 1802–2685 m (Fig. 4).

Lithology Stronger rocks give the driving forces more resistance, which makes them less susceptible to landslides (Kanungo et al. 2006). Factors such as the genetic type of rock, the nature and existence of discontinuities such as joints or other fractures, and the degree of weathering influence the strength of a rock (Ajin et al. 2016). The lithology of this district was extracted from the geological map of Kerala at 1:50,000 scale using ArcGIS tools. The rock types present in the study area are charnockite, granite, pink granite gneiss, hornblende gneiss, and garnet-biotite gneiss (Fig. 5). Around 52.42% of the district is comprised of gneissic rock types.

Land use/land cover types The land use/land cover of an area is one of the major factors responsible for slope
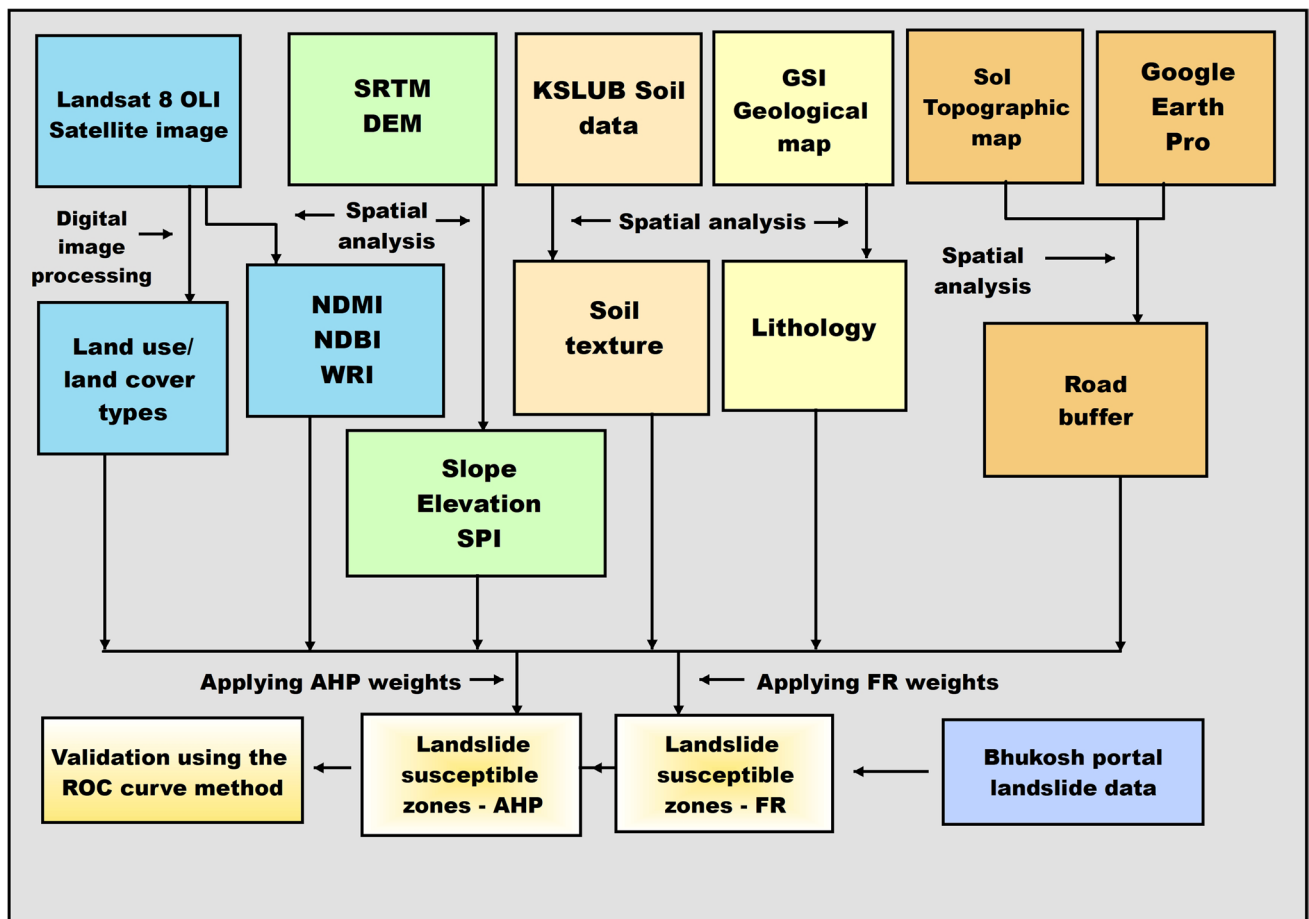

Fig. 2 The flowchart of the landslide modelling

Slope angle

Slope angle

[Natural breaks (Jenks) classification]

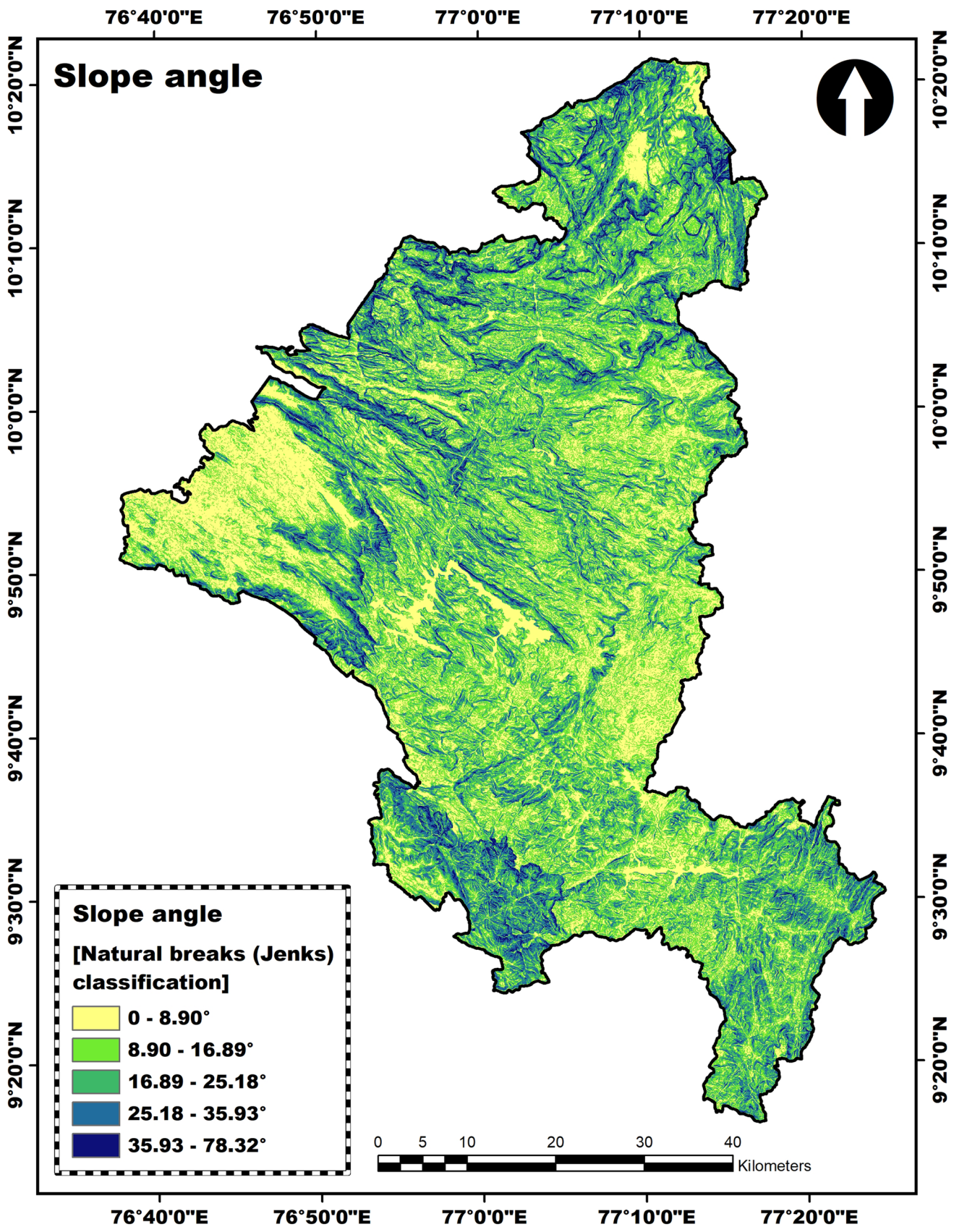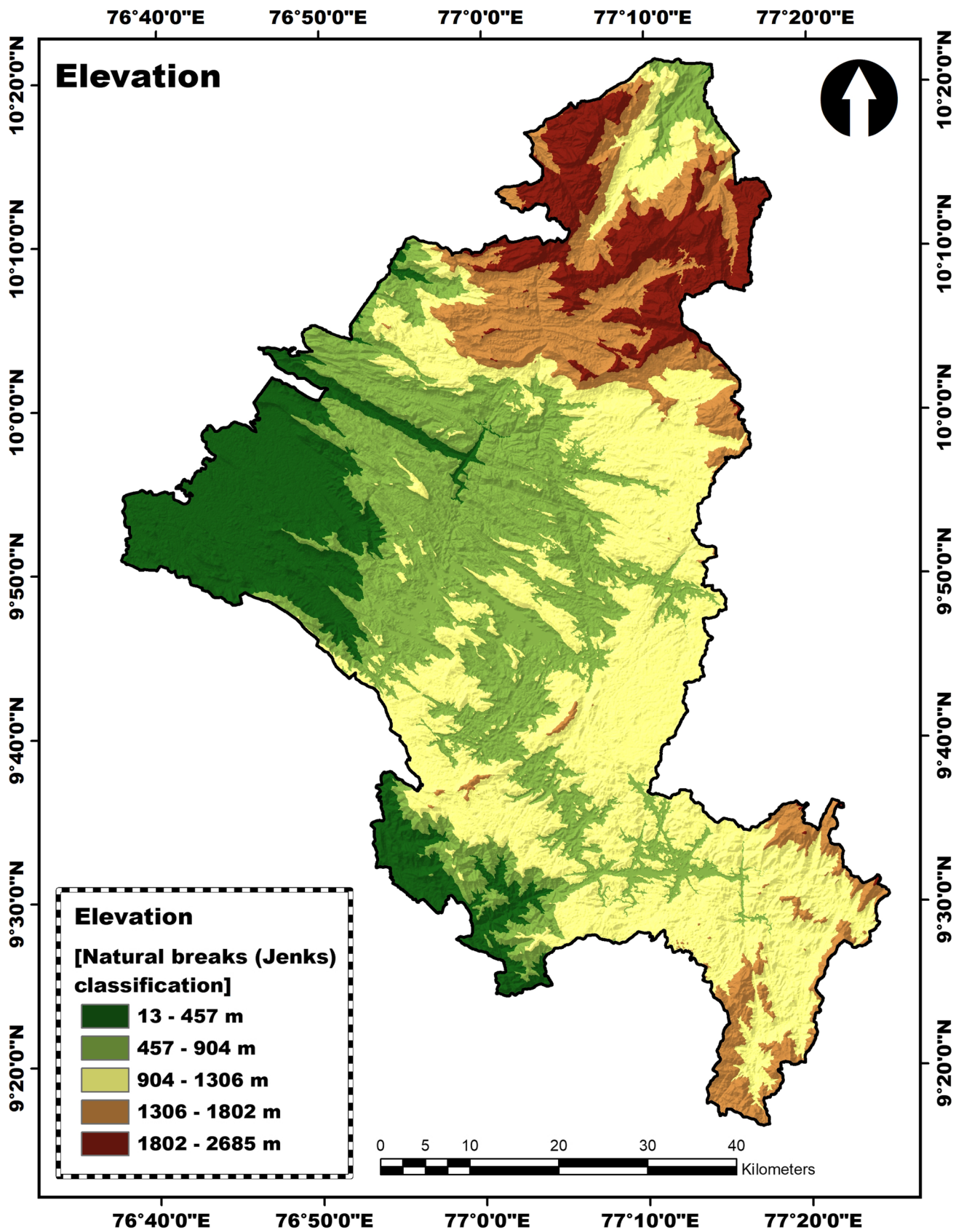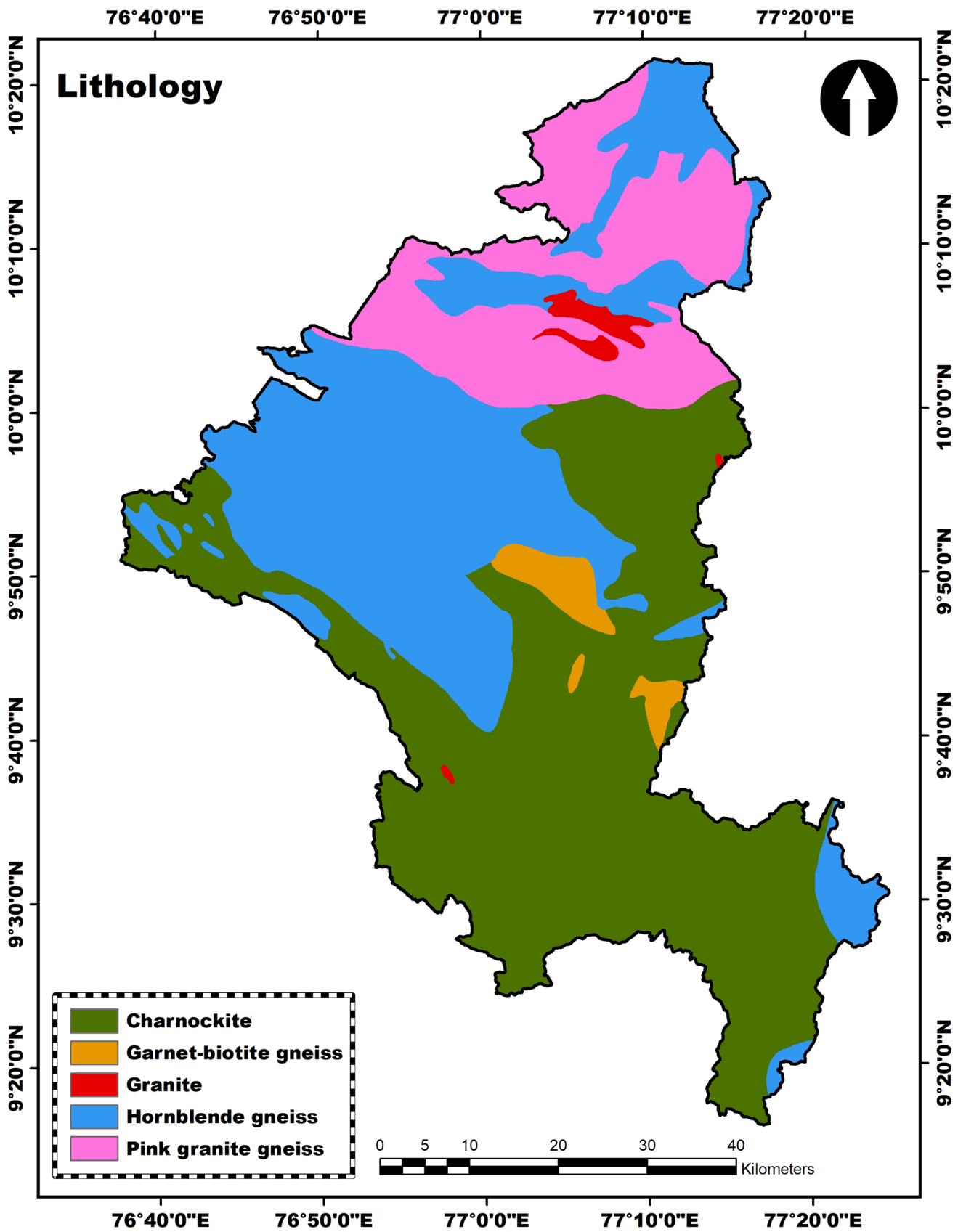|	
	0 - 8.90°
	8.90 - 16.89°
	16.89 - 25.18°
	25.18 - 35.93°
	35.93 - 78.32°

Fig. 3 Slope angle

Fig. 4 Elevation

Fig. 5 Lithology

instability. Forested areas are less prone to landslides compared to barren land. This is because vegetation with a strong root system stabilizes the slopes (García-Rodríguez et al. 2008) by binding the soil mass and thus increasing the shear strength of the soil (Turrini and Visintainer 1998). Areas with a high density of vegetation are able to sustain high water pressure during heavy precipitation (Oh et al. 2018), while barren and sparsely vegetated areas are vulnerable to weathering and instability in the slope (Anbalagan 1992). Land use plays a major role in the behavior of slopes by affecting the rate of infiltration of surface water during the rainy season (Ajin et al. 2016). Land cover change in the areas with higher slopes can result in landslides (Kanungo et al. 2009; Karsli et al. 2009).

Land use and land cover types were derived from the Landsat 8 OLI satellite image of 30-m spatial resolution. The supervised classification approach in the ERDAS Imagine software was used to classify the satellite image. The maximum likelihood (ML) classification method was applied to classify the land use/land cover types present in the district. The land use/land cover types present in the Idukki district are evergreen forest, deciduous forest, built-up area, water body, scrubland, cropland, plantation, and barren land (Fig. 6).

NDMI NDMI was derived from the Landsat 8 OLI satellite image using Eq. (1) (Gao 1996). The NDMI value ranges between -1 and $+1$ (Zhang et al. 2016). The higher NDMI indicates higher soil moisture, and lower NDMI indicates lower soil moisture content (Sar et al. 2015). The NDMI of the study area ranges from -0.38 to 0.37 (Fig. 7) and is grouped into five classes: -0.38 to -0.02, -0.02–0.05, 0.05–0.12, 0.12–0.17, and 0.17–0.37.

$$NDMI = \frac{(NIR - SWIR)}{(NIR + SWIR)} \tag{1}$$

The chance of landslides is high in areas with higher NDMI. This is because moisture can increase the pressure of the pore water and thus reduce the strength of the soil (Ray and Jacobs 2007).

Road buffer Roads are another important factor which causes instability on the slopes (Ortiz and Martínez-Graña 2018; Xie et al. 2018). The undercutting or excavation of slopes for road construction and the additional loads caused by the movement of vehicles can affect the slope equilibrium (Pourghasemi et al. 2012b). A road cutting can serve as a barrier, a net sink, a net source, or a water flow corridor (Pradhan and Lee 2010). This, in turn, may cause slope instability. The physiographic divisions of Kerala include the lowlands (< 7 m), the midlands (7–75 m), and the highlands (> 75 m) (Resmi et al. 2016). In this study, only the

road networks within the highlands of Idukki district were selected. Road networks were digitized from the topographic maps and Google Earth Pro, and with ArcGIS Spatial Analyst (proximity) tools, the 100-m buffer distance was generated (Fig. 8). About 17% of the study area falls within the 100-m buffer distance from roads.

NDBI NDBI is used to extract impervious surface (Shahfahad et al. 2020). NDBI was extracted from the Landsat 8 OLI satellite image using ArcGIS tools and Eq. (2) (Zha et al. 2003). The NDBI ranges between -1 and $+1$ (Ibrahim 2017). The NDBI of the study area is grouped into five classes: -0.37 to -0.18, -0.18 to -0.12, -0.12 to -0.05, -0.05–0.01, and 0.01–0.38 (Fig. 9).

$$NDBI = \frac{(SWIR - NIR)}{(SWIR + NIR)} \tag{2}$$

NDBI represents impervious surfaces such as roads and settlements, influencing water runoff (Pham et al. 2020) and these structures can decrease the stability of slopes. Hence, the chance of landslides is high in areas with high NDBI.

WRI WRI was derived from the Landsat 8 OLI satellite images using ArcGIS tools and Eq. (3) (Shen and Li 2010). The WRI of this district ranges from 0.07 to 1.33 (Fig. 10) and is grouped into five classes (0.07–0.60, 0.60–0.64, 0.64–0.69, 0.69–0.86, and 0.86–1.33).

$$WRI = \frac{(Green + Red)}{(NIR + SWIR)} \tag{3}$$

The WRI above 1 represents water (Shen and Li 2010). Hence, the likelihood of landslides is more on slopes with WRI below 1, as these slopes will be more saturated.

SPI SPI is an erosive water flow power measurement and was calculated using Eq. (4) (Moore et al. 1991). The SPI of this area has been generated from the DEM using spatial analyst tools, and the value ranges between -31.32 and 14.84 (Fig. 11):

$$SPI = \alpha \tan \beta \tag{4}$$

where α is the specific catchment area ($A = A/L$, catchment area (A) divided by contour length (L)] and β is the local slope.

The probability of landslides is high in areas with higher SPI. This is because streams can negatively affect the stability of the slope (Ortiz and Martínez-Graña 2018) by undercutting and eroding the slopes (Chen et al. 2018; Elmoulat and Ait Brahim 2018; Sifa et al. 2019) or saturating the lower part of slopes (Chen et al. 2018). The increase in the pore water pressure due to water infiltration reduces the

Fig. 6 Land use/land cover types
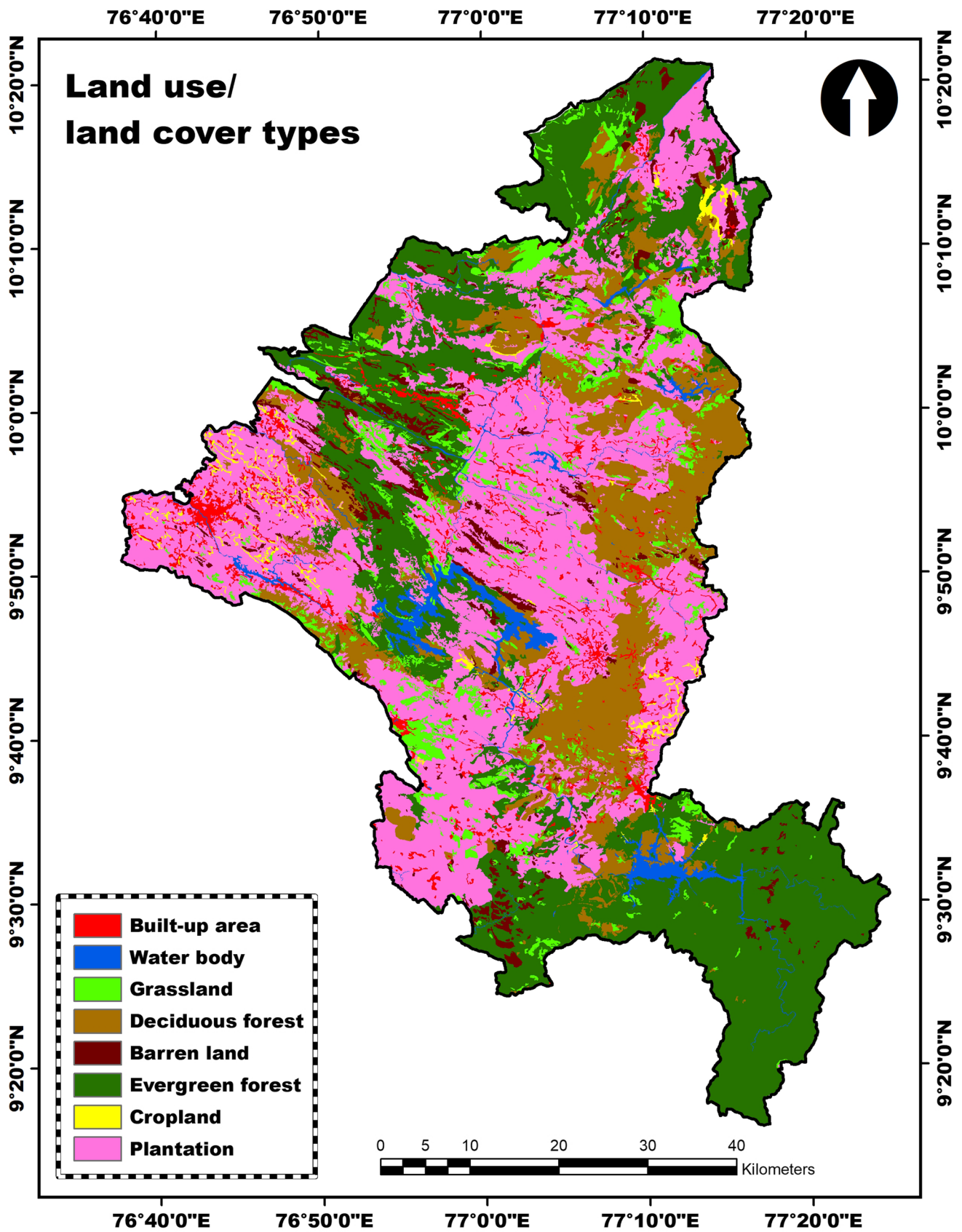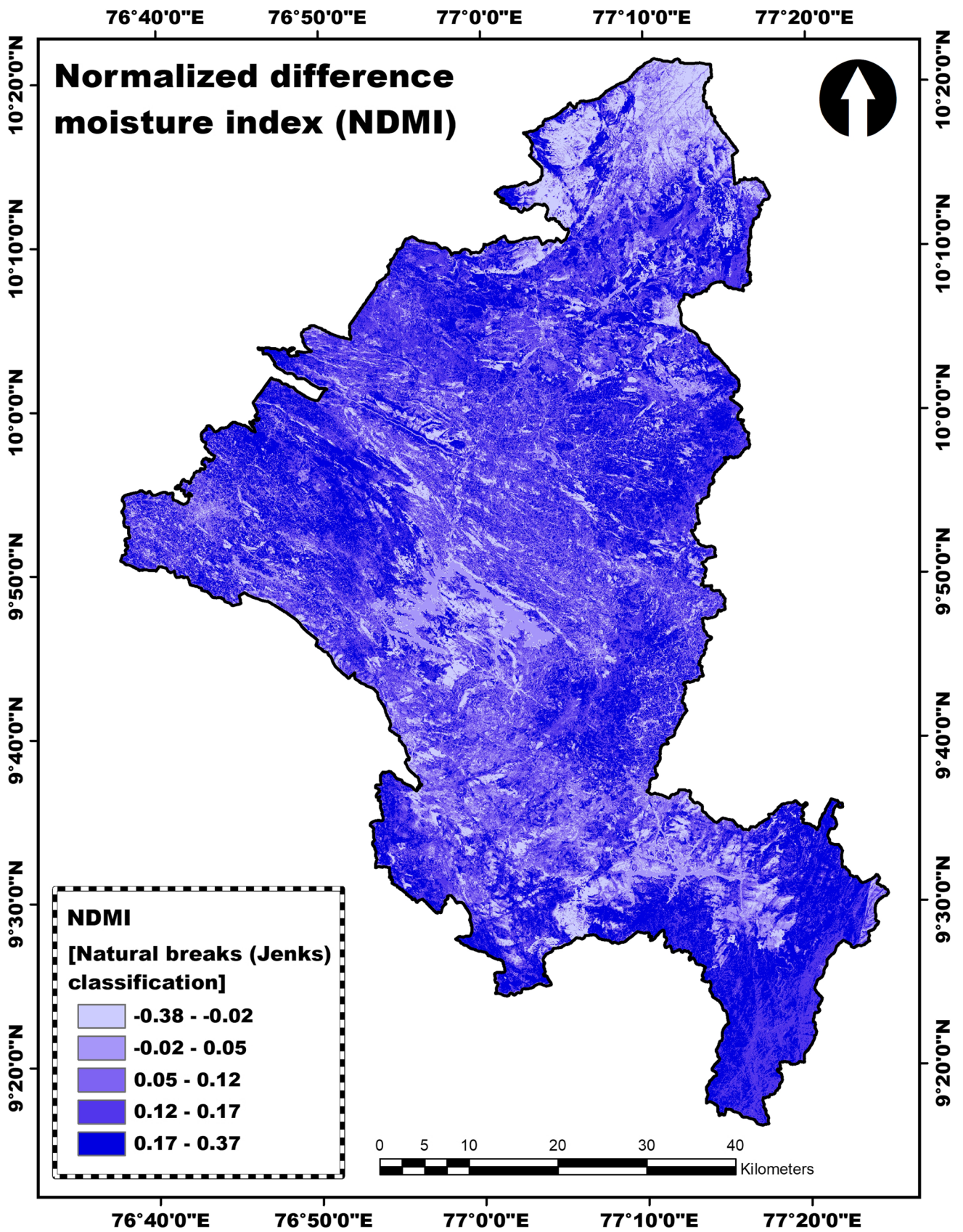
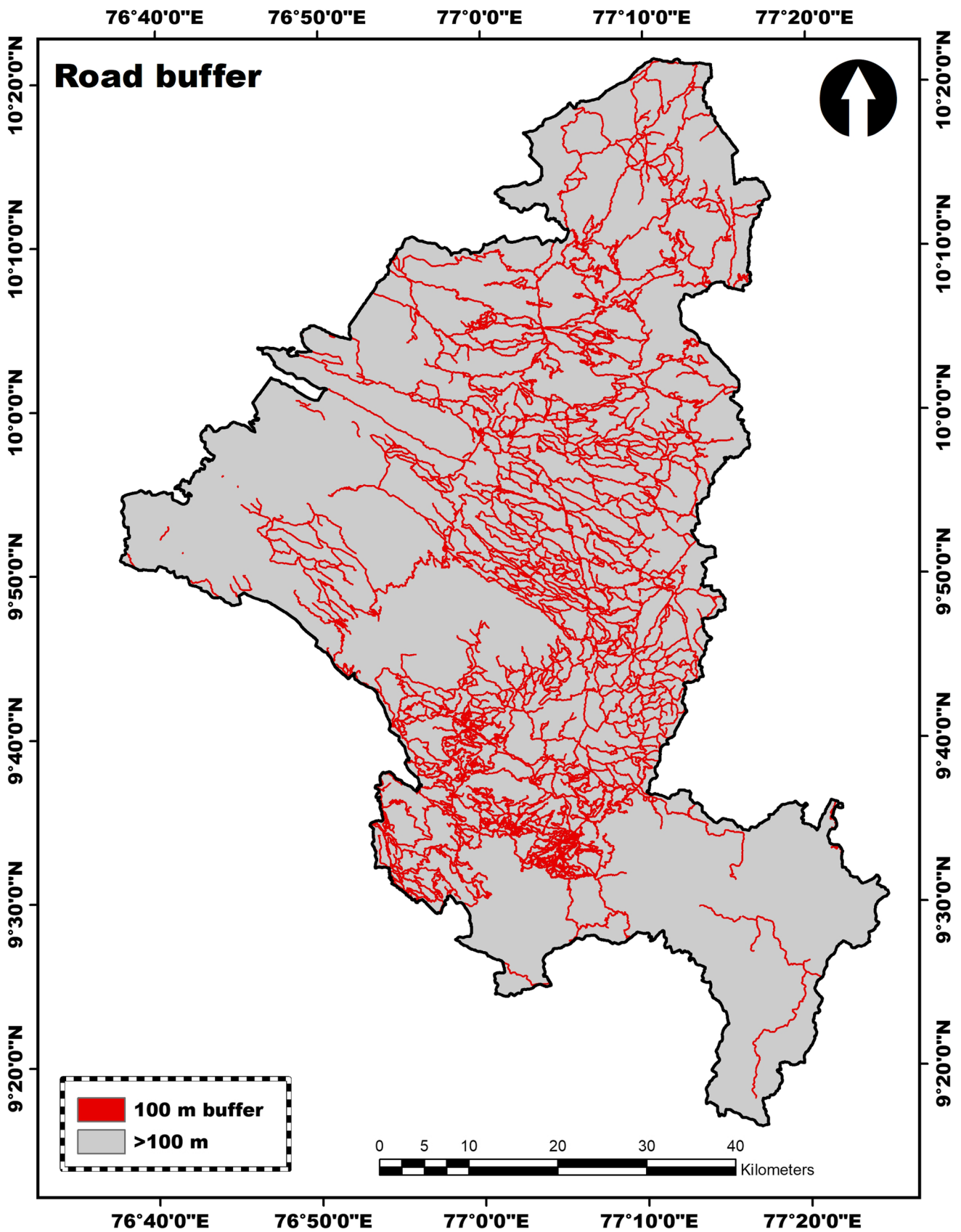**Fig. 7** Normalized difference moisture index
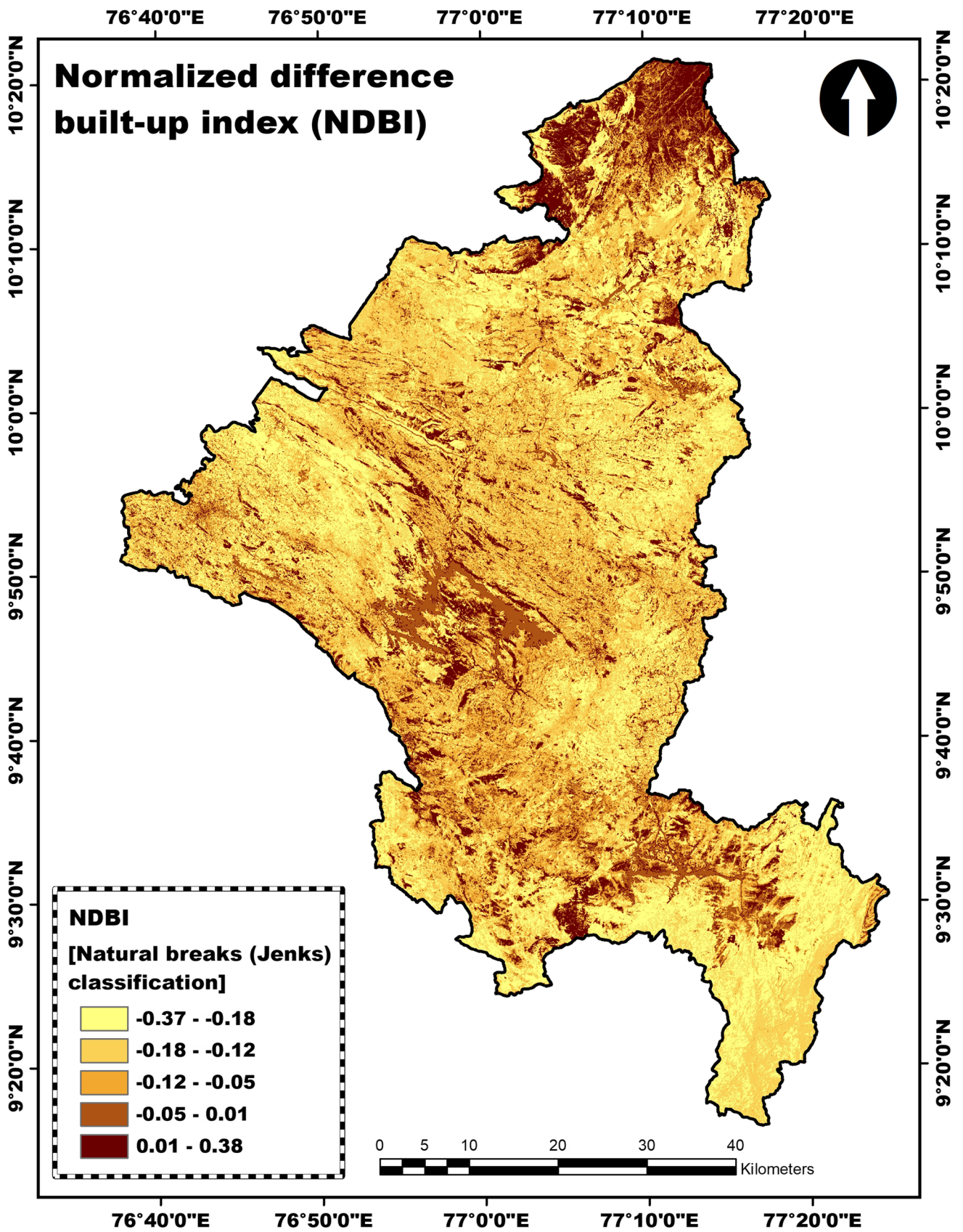
Fig. 8 Road buffer

Fig. 9 Normalized difference built-up index

Fig. 10 Water ratio index

Stream power index (SPI)

SPI

[Natural breaks (Jenks) classification]

- ▓ -31.32 - -4.89
- ▓ -4.89 - -2.35
- ▓ -2.35 - -0.72
- ░ -0.72 - 0.53
- ░ 0.53 - 14.84
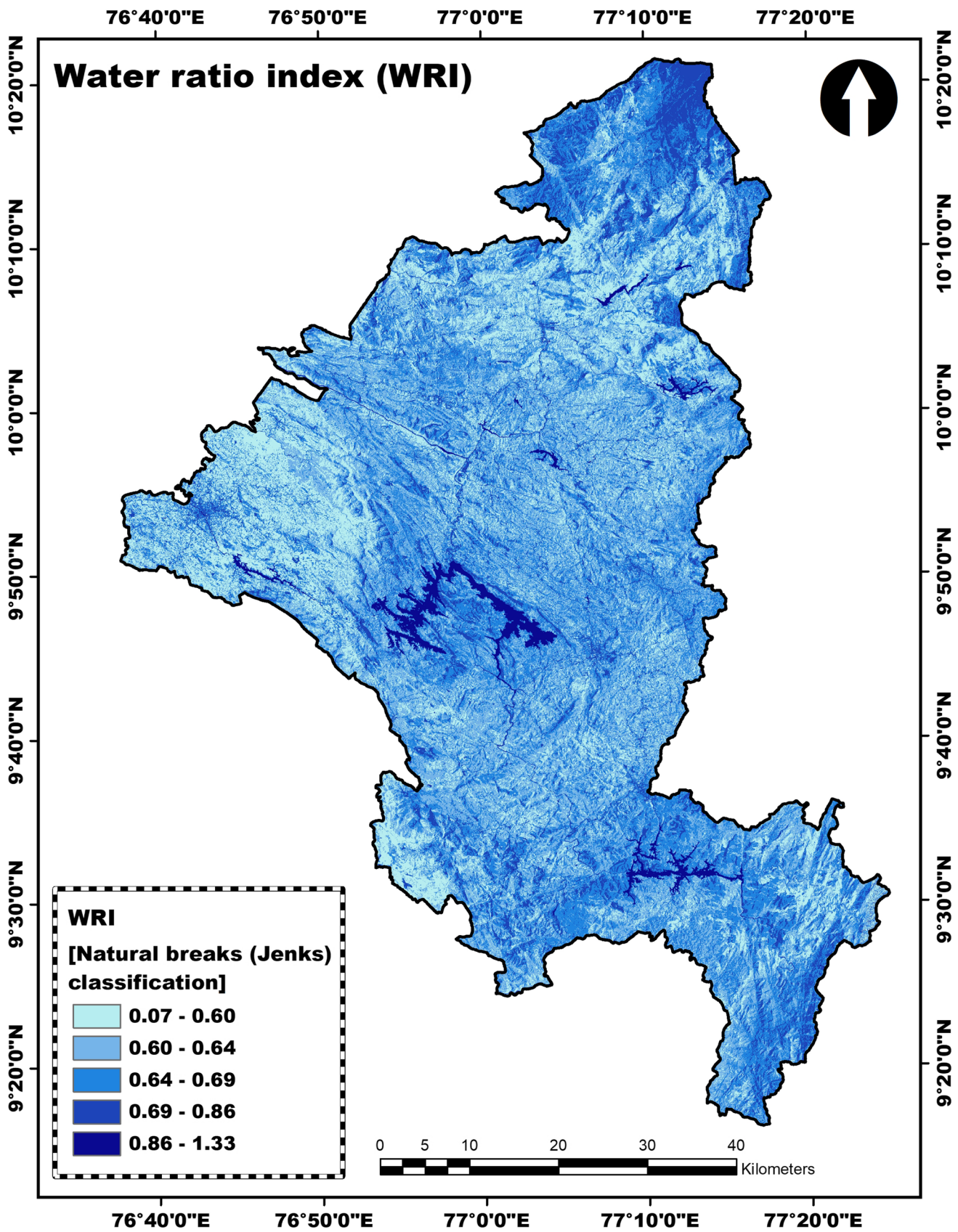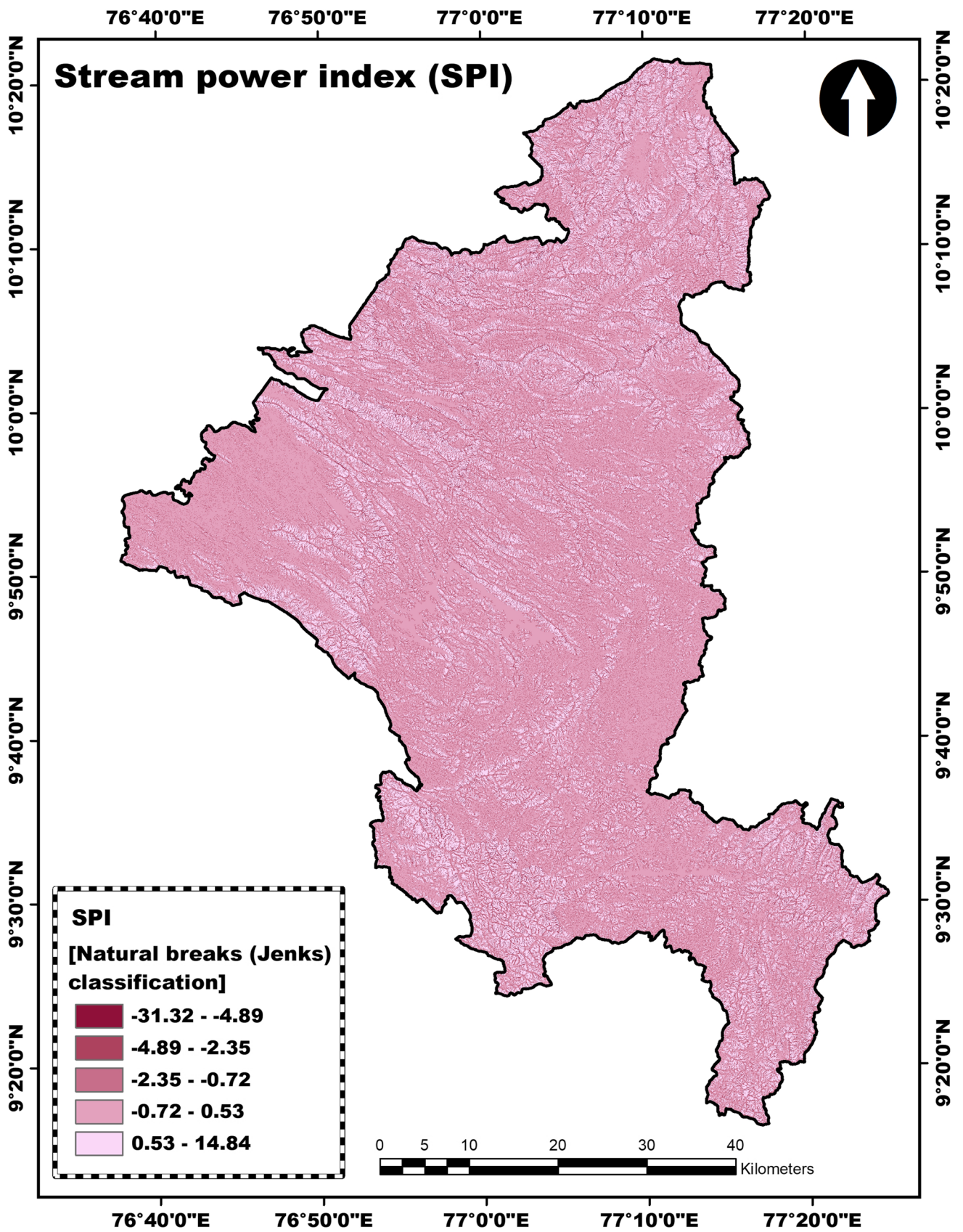
Fig. 11 Stream power index
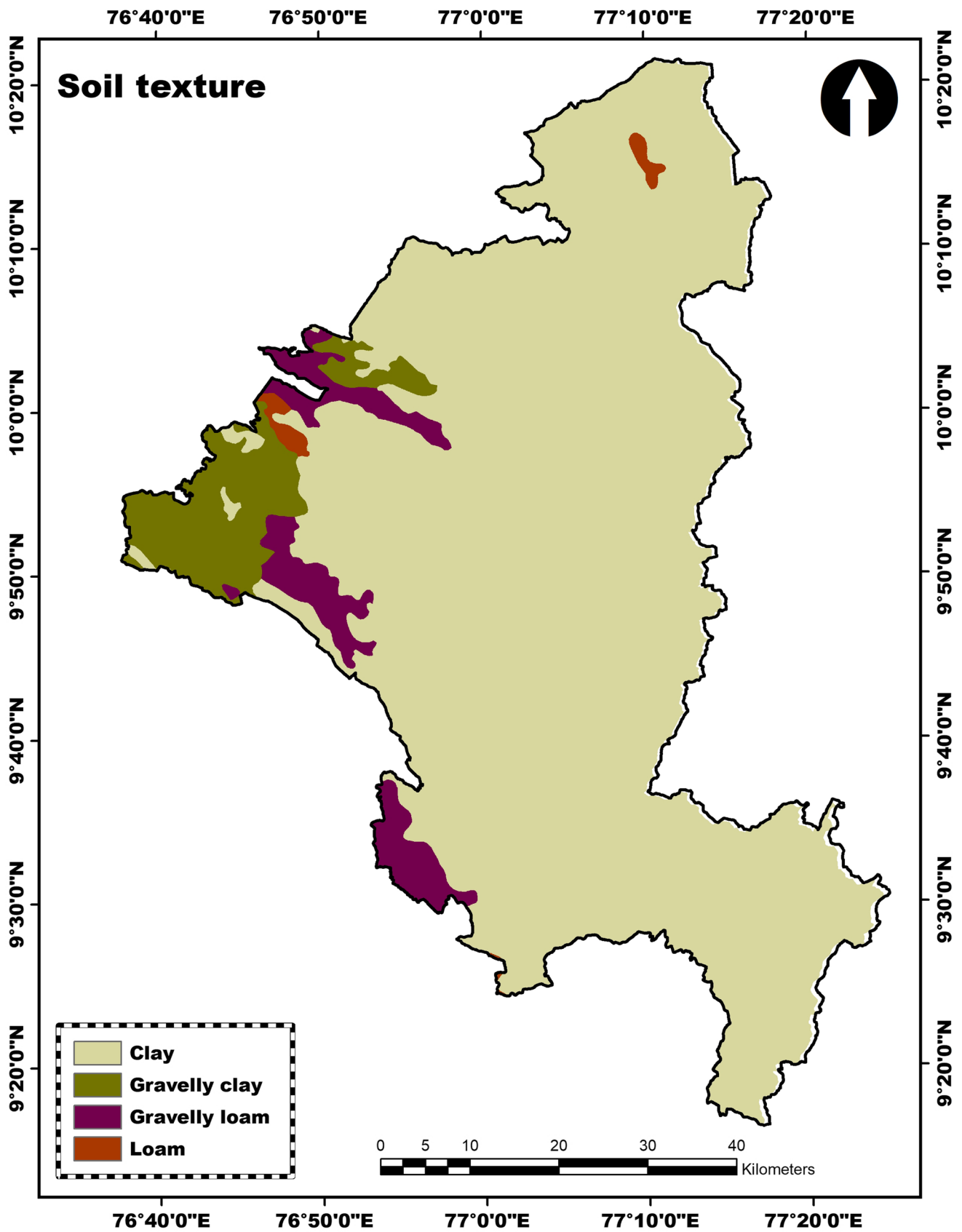
Fig. 12 Soil texture

Table 1 Pairwise comparison matrix

	Slp	Ele	Litho	LULC	NDMI	RB	NDBI	WRI	SPI	Soil	Vp	Cp
Slp	1	2	3	4	5	6	7	8	9	10	4.529	0.291
Ele	1/2	1	2	3	4	5	6	7	8	9	3.356	0.216
Litho	1/3	1/2	1	2	3	4	5	6	7	8	2.414	0.155
LULC	1/4	1/3	1/2	1	2	3	4	5	6	7	1.707	0.110
NDMI	1/5	1/4	1/3	1/2	1	2	3	4	5	6	1.196	0.077
RB	1/6	1/5	1/4	1/3	1/2	1	2	3	4	5	0.836	0.054
NDBI	1/7	1/6	1/5	1/4	1/3	1/2	1	2	3	4	0.586	0.038
WRI	1/8	1/7	1/6	1/5	1/4	1/3	1/2	1	2	3	0.414	0.027
SPI	1/9	1/8	1/7	1/6	1/5	1/4	1/3	1/2	1	2	0.298	0.019
Soil	1/10	1/9	1/8	1/7	1/6	1/5	1/4	1/3	1/2	1	0.221	0.014
$\sum$	**2.93**	**4.83**	**7.72**	**11.59**	**16.45**	**22.28**	**29.08**	**36.83**	**45.50**	**55.00**	**15.56**	**1.00**

soil's shear strength and leads to slope failure (Chawla et al. 2018; Sifa et al. 2019).

Soil Clay is the soil type with high porosity and low permeability and hence holds more water. The increase in pore water pressure decreases the soil's shear strength and results in a slope failure (Chawla et al. 2018). Thus, clay acts as the potential slip zone causing landslides (Sartohadi et al. 2018). The shape file of soil data at 1:250,000 scale was collected from the KSLUB. The soil types present in the study area are clay, gravelly clay, loam, and gravelly loam (Fig. 12). Clayey soil makes up approximately 88% of the study area.

AHP Modelling

The AHP method (Saaty 1980) is a decision-making tool developed to evaluate complex multi-criteria alternatives (Emrouznejad and Marra 2017). AHP can hierarchically calculate and synthesize a variety of factors of a complex decision and making it simple and easy to integrate (Russo and Camanho 2015). This method assigns reasonable weights to variables under consideration owing to its unique consistency test (Devara et al. 2021).

The processes involved in the AHP modelling include construction of a pair-wise comparison matrix, calculation of eigen vector, and weighting coefficient (Table 1), and calculation of eigen value, consistency index, and consistency ratio (Table 2). Equations (5) and (6) determined eigen vector (Vp) and weighting coefficient (Cp) (Danumah et al. 2016). Equations (7), (8), and (9) were used to determine the eigen value (λmax), consistency index (CI), and consistency ratio (CR) (Danumah et al. 2016). The major steps involved in AHP modelling are included in Fig. 13.

where *Slp.* = slope angle; *Ele.* = elevation, *Litho.* = lithology, and *RB* = road buffer.

$$Vp = \sqrt[k]{W1x \dots Wk} \tag{5}$$

where k = number of factors and W = ratings of the factors.

$$Cp = \frac{Vp}{Vp1 + \dots Vpk} \tag{6}$$

$$\lambda max = \frac{[E]}{k} \tag{7}$$

$$CI = (\lambda max - k)/(k - 1) \tag{8}$$

$$CR = \frac{CI}{RI} \tag{9}$$

where RI is the random index (Table 3).

According to Saaty (1980), the CR should not exceed 10% (0.1). If the CR exceeds 10%, the judgments are inconsistent and the subjective judgments need to be revised.

The landslide susceptible zones were derived using Eq. (10).

$$
\begin{aligned}
LSZ = {} & (0.291 \times Slp.) + (0.216 \times Ele.) \\
& + (0.155 \times Litho.) + (0.110 \times LULC) \\
& + (0.077 \times NDMI) + (0.054 \times RB) + (0.038 \times NDBI) \\
& + (0.027 \times WRI) \\
& + (0.019 \times SPI) + (0.014 \times Soil)
\end{aligned} \tag{10}
$$

FR Modelling

The FR model shows the correlation between the landslide locations and the factors, based on the relationship found between landslide distribution and each causative factors (Lee and Pradhan 2006). To calculate the frequency ratio

Table 2 Normalized matrix

	Slp	Ele	Litho	LULC	NDMI	RB	NDBI	WRI	SPI	Soil	∑ rank	[C]	[D]=[A]*[C]	[E]=[D]/[C]	λmax	CI	CR
Slp	0.34	0.41	0.39	0.35	0.30	0.27	0.24	0.22	0.20	0.18	2.90	0.290	3.177	10.954	**10.547**	**0.061**	**0.041**
Ele	0.17	0.21	0.26	0.26	0.24	0.22	0.21	0.19	0.18	0.16	2.10	0.210	2.322	11.061			
Litho	0.11	0.10	0.13	0.17	0.18	0.18	0.17	0.16	0.15	0.15	1.52	0.152	1.668	11.009			
LULC	0.09	0.07	0.06	0.09	0.12	0.13	0.14	0.14	0.13	0.13	1.09	0.109	1.185	10.830			
NDMI	0.07	0.05	0.04	0.04	0.06	0.09	0.10	0.11	0.11	0.11	0.79	0.079	0.834	10.586			
RB	0.06	0.04	0.03	0.03	0.03	0.04	0.07	0.08	0.09	0.09	0.56	0.056	0.583	10.341			
NDBI	0.05	0.03	0.03	0.02	0.02	0.02	0.03	0.05	0.07	0.07	0.40	0.040	0.407	10.157			
WRI	0.04	0.03	0.02	0.02	0.02	0.01	0.02	0.03	0.04	0.05	0.28	0.028	0.286	10.084			
SPI	0.04	0.03	0.02	0.01	0.01	0.01	0.01	0.01	0.02	0.04	0.20	0.020	0.206	10.145			
Soil	0.03	0.02	0.02	0.01	0.01	0.01	0.01	0.01	0.01	0.02	0.15	0.015	0.156	10.299			
∑	1.00	1.00	1.00	1.00	1.00	1.00	1.00	1.00	1.00	1.00	10.00	1.000		105.465			

for each class of the causative factors, the following equation (Ehret et al. 2010) was used:

$$FR = \left(\frac{Mi}{M}\right) \Big/ \left(\frac{Ni}{N}\right) \tag{11}$$

where Mi is the number of landslide pixels for each factor class, M is the number of landslides within the study area, Ni is the number of pixels for each factor class, and N is the number of pixels in total for the study area. (Ehret et al. 2010). When the FR value is more than 1, a high likelihood of landslides and higher correlations is inferred, whereas values less than 1 imply a lower correlation (Lee and Talib 2005). The frequency ratio of each class is shown in Table 4.

The landslide susceptible zones were derived using Eq. (12).

$$\begin{aligned} LSZ \; &= Fr(Slp.) + Fr(Ele.) \\ &\quad + Fr(Litho.) + Fr(LULC) + \; Fr(NDMI) \\ &\quad + Fr(RB) + Fr(NDBI) + Fr(WRI) + Fr(SPI) + Fr(Soil) \end{aligned} \tag{12}$$

Validation Using the ROC Curve Method

The ROC curve method was used to validate the landslide susceptibility maps created using the AHP and FR methods. For validating the maps, the landslide incidence data collected from the Bhukosh portal of GSI was used. A total of 1304 landslide incidences have been recorded in this district. These incidences have been randomly split into a training dataset with 913 landslides (70% of the incidences) and a validation dataset consists of 391 landslides (30% of the incidences). The validation dataset was used to validate the results using the ROC curve method. RStudio was used to plot the ROC curves and to estimate the AUC values. The value of the AUC varies from 0.5 to 1.0, where the lowest value indicates random classification, while the highest value represents an excellent classification (Melo 2013). The AUC value ranges and corresponding discriminations are included in Table 5.

Results and Discussion

This study demarcated landslide susceptible zones in the Idukki district using the AHP and FR methods. The very high susceptible zone covers 11.14% of the study area using the AHP model, and 6.57% using the FR model. The area of the district is grouped into five susceptible zones, and the area of each susceptible zone is mentioned in Table 6. The number and percentage of landslide incidences in each susceptible zone are shown in Table 7.
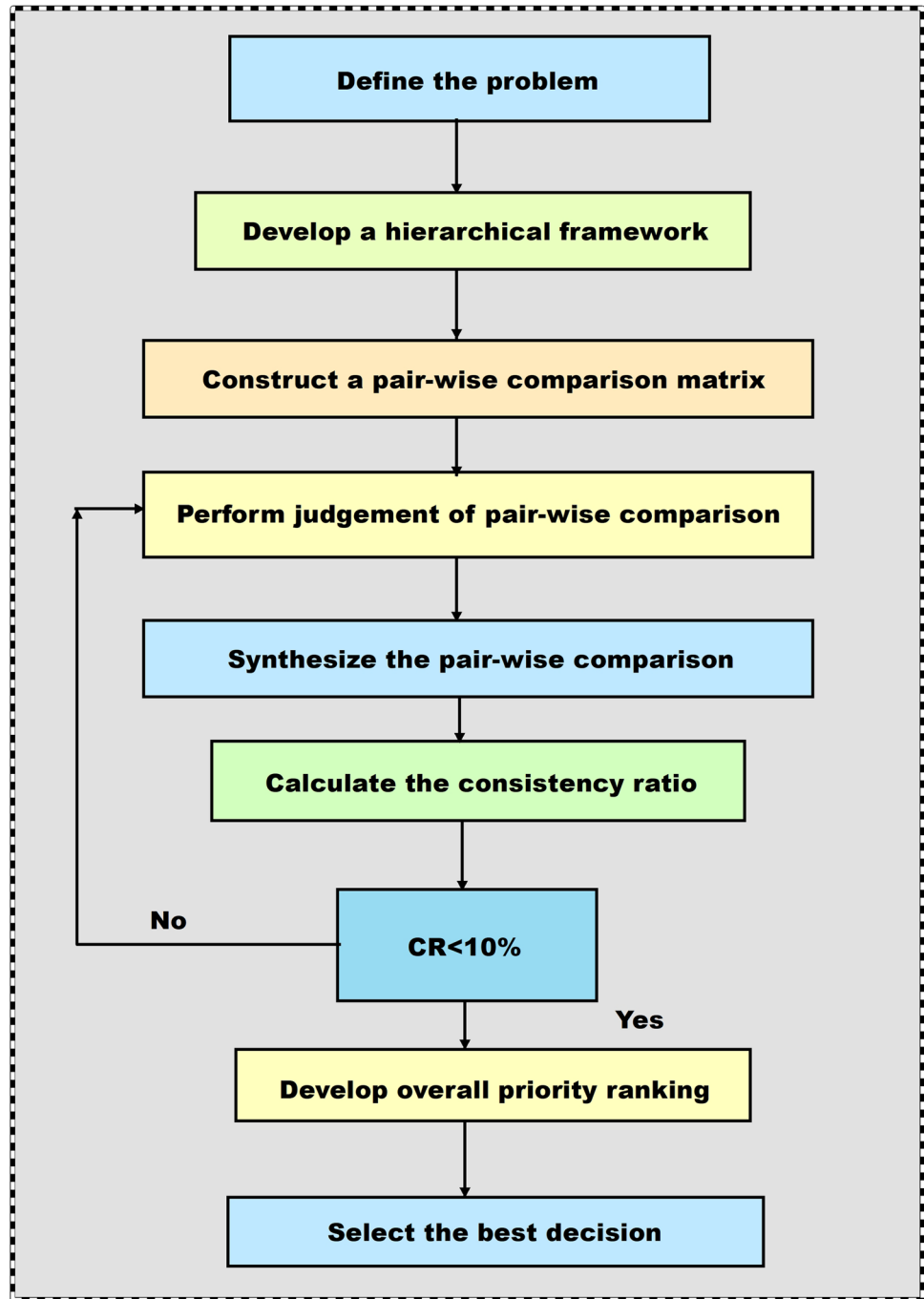
Fig. 13 Flowchart of the AHP modelling

Number of factors	2	3	4	5	6	7	8	9	10	11
RI	0.00	0.58	0.90	1.12	1.24	1.32	1.41	1.45	1.49	1.51

About 71% of the landslides occurred in the high and very high susceptible zones for the AHP method, whereas 77.75% occurred in those zones for the FR method. The prepared landslide susceptibility maps are depicted in Figs. 14 and 15. This study confirmed that gravelly loam soil, followed by NDBI ranging between 0.01 and 0.38, elevation ranging between 457 and 904 m, hornblende gneiss rock type, built-up and plantation areas, slope ranging between 16.89 and 35.93°, road cuttings, and WRI ranging between 0.69 and 0.86 are the major landslide-inducing factors in Idukki

Table 4 The frequency ratio of each classes

Sl. No	Factors	Class	No. of pixels in the class	Class (%)	Number of landslide pixels within the class	Landslide incidences (%)	Frequency ratio
1	Slope	0–8.90°	1,210,793	24.96	58	6.35	0.25
		8.90–16.89°	1,522,708	31.39	211	23.11	0.73
		16.89–25.18°	1,202,061	24.78	405	44.36	1.79
		25.18–35.93°	739,767	15.25	226	24.75	1.62
		35.93–78.32°	175,604	3.62	13	1.42	0.39
2	Elevation	13–457 m	722,304	14.89	68	7.45	0.50
		457–904 m	1,413,077	29.13	627	68.67	2.36
		904–1306 m	1,735,179	35.77	136	14.89	0.41
		1306–1802 m	608,307	12.54	77	8.43	0.67
		1802–2685 m	372,066	7.67	5	0.55	0.07
3	Lithology	Charnockite	2,259,565	46.58	144	15.77	0.34
		Granite	48,509	1	18	1.97	1.97
		Pink granite gneiss	826,598	17.04	96	10.51	0.61
		Garnet-biotite gneiss	102,356	2.11	18	1.97	0.93
		Hornblende gneiss	1,613,905	33.27	637	69.77	2.10
4	LULC	Water body	125,639	2.59	0	0	0.00
		Evergreen forest	1,543,082	31.81	157	17.19	0.54
		Deciduous forest	772,269	15.92	99	10.84	0.68
		Scrubland	300,273	6.19	69	7.56	1.22
		Barren land	172,693	3.56	12	1.31	0.37
		Cropland	48,994	1.01	2	0.22	0.22
		Built-up area	173,178	3.57	61	6.69	1.87
		Plantation	1,714,805	35.35	513	56.19	1.59
5	NDMI	−0.38 to −0.02	400,688	8.26	44	4.82	0.58
		−0.02–0.05	669,429	13.8	246	26.94	1.95
		0.05–0.12	911,005	18.78	349	38.22	2.03
		0.12–0.17	1,473,713	30.38	212	23.22	0.76
		0.17–0.37	1,396,098	28.78	62	6.79	0.23
6	Road buffer	0–100 m	824,644	17	247	27.05	1.59
		More than 100 m	4,026,289	83	666	72.94	0.88
7	NDBI	−0.37 to −0.18	1,184,598	24.42	242	26.5	1.08
		−0.18 to −0.12	1,628,458	33.57	50	5.47	0.16
		−0.12 to −0.05	939,141	19.36	47	5.15	0.26
		−0.05–0.01	660,697	13.62	219	23.98	1.76
		0.01–0.38	438,039	9.03	355	38.88	4.3
8	WRI	0.07–0.60	862,012	17.77	163	17.85	1
		0.60–0.64	1,853,541	38.21	309	33.84	0.88
		0.64–0.69	1,565,396	32.27	320	35.05	1.08
		0.69–0.86	489,459	10.09	121	13.25	1.31
		0.86–1.33	80,525	1.66	0	0	0
9	SPI	−31.32 to −4.80	38,807	0.8	3	0.33	0.41
		−4.89 to −2.35	355,088	7.32	94	10.29	1.4
		−2.35 to -0.72	809,136	16.68	83	9.09	0.54
		−0.72–0.53	2,852,349	58.8	523	57.28	0.97
		0.53–14.84	795,553	16.4	210	23	1.4
10	Soil	Gravelly loam	31,046	0.64	27	2.96	4.62
		Loam	240,606	4.96	4	0.44	0.09
		Gravelly clay	306,579	6.32	48	5.26	0.83
		Clay	4,272,702	88.08	834	91.35	1.03

Table 5 AUC values and discrimination (Source: Li and He 2018)

Sl. No	AUC value	Discrimination
1.	0.9–1.0	Excellent
2.	0.8–0.9	Good
3.	0.7–0.8	Fair
4.	0.6–0.7	Poor
5.	0.5–0.6	Fail

district. The study area's middle portion shows very high susceptibility to landslides due to steeper slopes, proximity to streams, and the presence of roads with vertical cuts. Most of the landslides occurred on this portion of the district.

The FR of 1.79 and 1.62 confirmed that the probability of landslide occurrences is high in areas with moderate slopes ranging between 16.89–25.18° and 25.18–35.93°. The lower FR (0.39) indicates lower landslide probability in areas with slopes above 35°. In their study, Nakileza and Nedala (2020) also found slopes ranging between 15 and 25° as the most influencing factor in landslide occurrence. Huang et al. (2018) found that the high and very high landslide suscepti-ble zones in the Nantian area of China are mainly distributed in areas with slopes ranging from 7.68 to 34.70°. Most of the landslides (627) occurred in areas with an elevation ranging from 457 to 904 m with a FR of 2.36. Also, the number of

landslides significantly decreases as the elevation increases above 904 m. This was confirmed after analyzing the num-ber of landslides recorded within higher elevation classes (904–1306 m, 1306–1802 m, and 1802–2685 m).

Nakileza and Nedala (2020) found that most of the land-slides occurred between elevations ranging from 1500 to 1800 m. Around 70% of the landslides occurred in areas with hornblende gneiss rock type. More than 500 landslides have been recorded in plantation areas. Among the land use land cover types, the built-up area (with a FR of 1.87) followed by plantation area (FR = 1.59) has a high correla-tion with landslide occurrences. The hill-toe modified for infrastructure development without any lateral support and slopes modified for monoculture plantations without proper drainage provisions are the causes of landslides in the Idukki district (Abraham et al. 2019).

Road cuttings with a FR of 1.59 indicate a higher prob-ability of landslides. The vertical cuts along the hilly roads in Idukki district make these roads susceptible to cut slope failures (Abraham et al. 2019). Sujatha and Sridhar (2021) found that around 74% of the landslides occurred in Coonoor due to road cuttings. The areas with positive NDBI (0.01–0.38) have the highest correlation with the landslide occurrence (FR = 4.3). Like this study, Huang et al. (2018) also found that landslide occurrence is high in areas with high NDBI.

Table 6 Area and percentage of landslide susceptible zones

Susceptible zones	AHP method		FR method	
	Area of susceptible zones (Sq. km)	Percentage of the area of the land-slide susceptible zones	Area of susceptible zones (Sq. km)	Percentage of the area of the landslide susceptible zones
Very low	468.49	10.75	872.47	20.02
Low	1035.46	23.76	1296.50	29.75
Moderate	1315.68	30.19	1143.98	26.25
High	1052.89	24.16	758.73	17.41
Very high	485.48	11.14	286.32	6.57
Total	**4358**	**100**	**4358**	**100**

Table 7 Number and percentage of landslide incidences in each susceptible zone

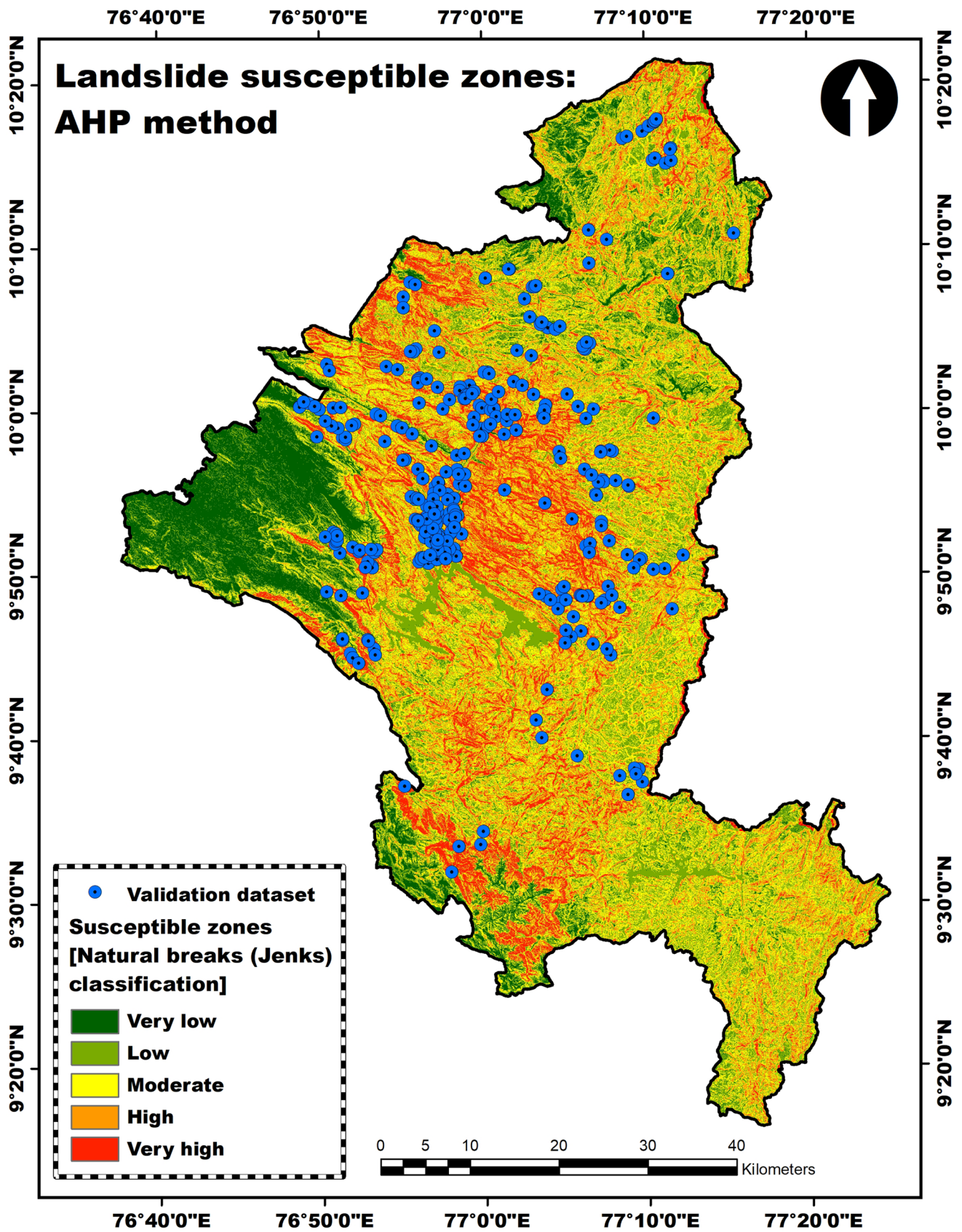| Susceptible zones	AHP method		FR method	
	Number of land-slide incidences	Percentage of land-slide incidences	Number of land-slide incidences	Percentage of landslide inci-dences
Very low	3	0.77	5	1.28
Low	38	9.72	26	6.65
Moderate	72	18.41	56	14.32
High	146	37.34	135	34.53
Very high	132	33.76	169	43.22
Total	**391**	**100**	**391**	**100**

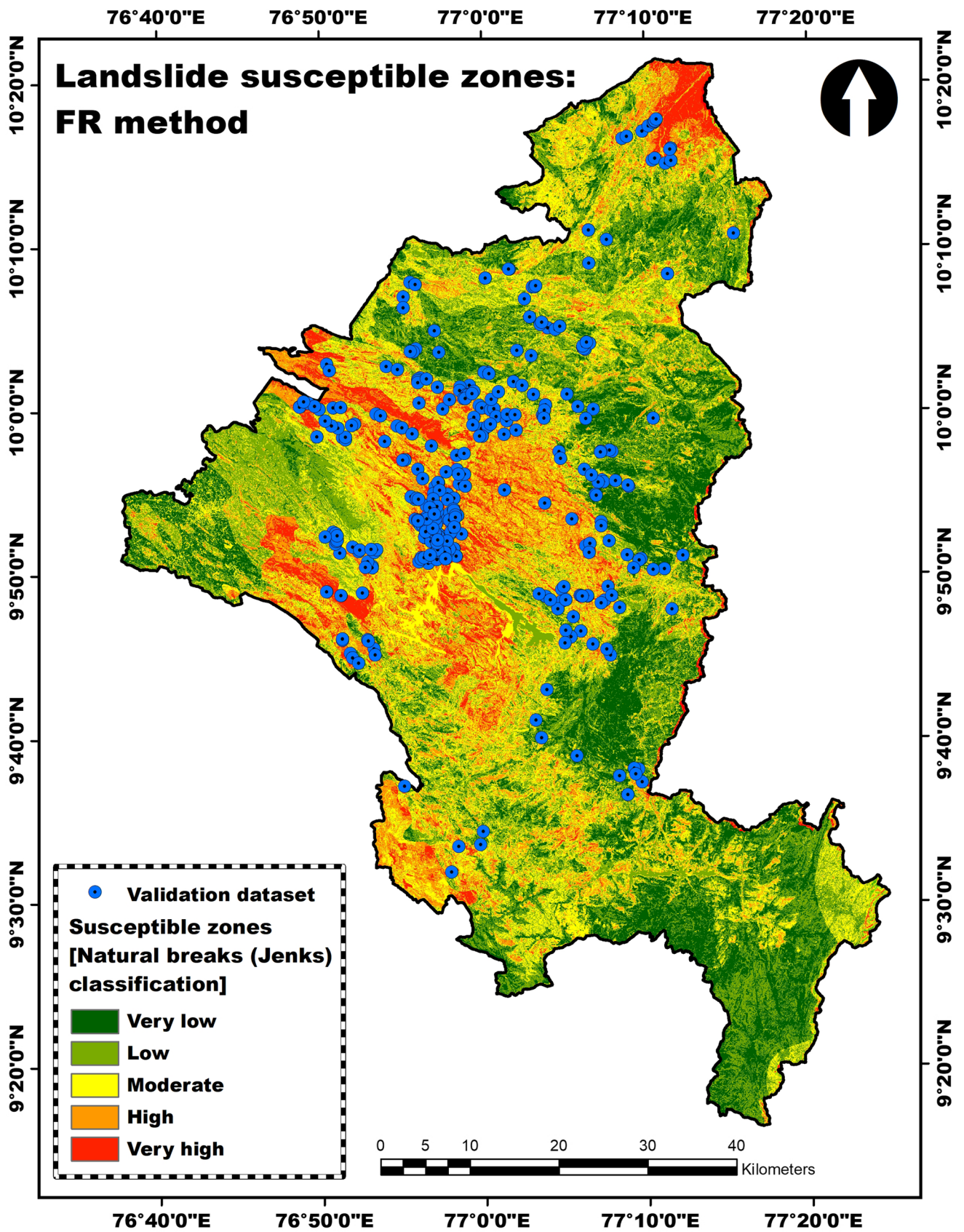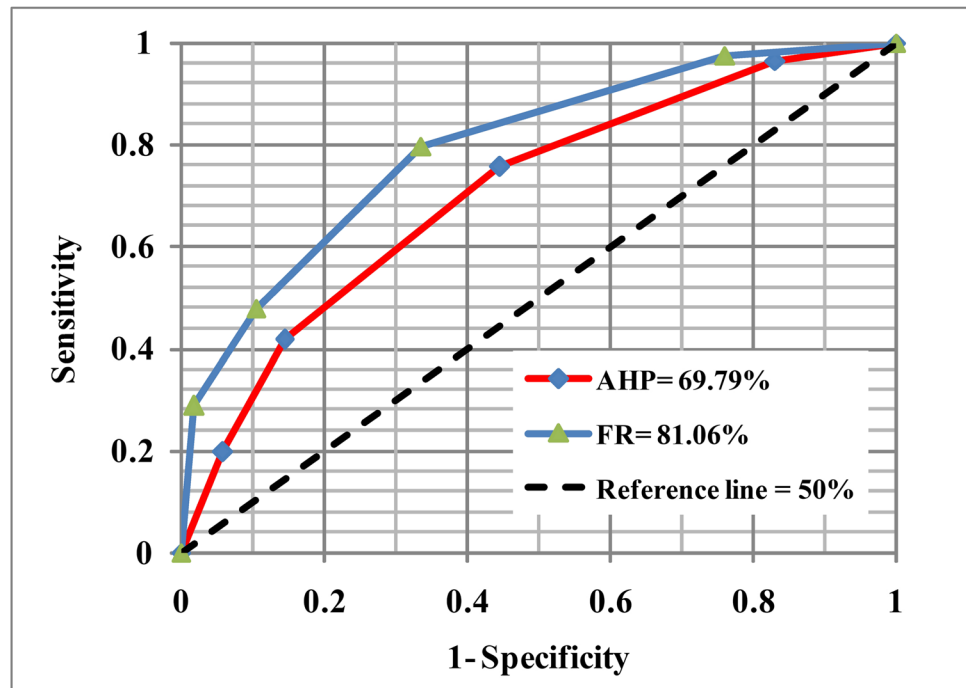**Fig. 14** Landslide susceptible zones: AHP method

Fig. 15 Landslide susceptible zones: FR method

Fig. 16 The ROC curves

Landslide occurrence in this district is highly correlated with the soil saturation. The FR (1.31) of the WRI class ranging between 0.69 and 0.86 confirmed this correlation. Though the number of landslides occurred in areas with clayey soil is 834 (91.34%), the FR (1.03) is much less than that of gravelly loam with a FR of 4.62. This is due to the fact that clayey soil accounts for approximately 88% of the district's land area. In their study, Roy and Saha (2019) found 15.79% of landslide areas in gravelly loam soil.

The AUC values estimated through the ROC curve method (Fig. 16) confirmed that the FR method is more effective in identifying landslide susceptible zones than the AHP method (Li and He 2018). The AUC value for the FR method is 0.81, which is considered good, while the AUC value for the AHP method (0.69) is considered poor. Thus, it is confirmed that the FR method is more suitable for landslide susceptibility modelling in the Idukki district and has thus been chosen as the best method. In their study, Kumar and Annadurai (2015), and Demir et al. (2013) also found the FR method as more effective than the AHP method in landslide susceptibility modelling. The geological structures (joints, faults, and shear zones) were not considered in this study due to the non-availability of data. This is a limitation of this study.

Conclusions

In this study, landslide susceptible zones in the Idukki district, the most landslide-prone district in Kerala, were delineated using the AHP and FR methods. The factors used to model landslide susceptibility were slope angle, elevation, lithology, LULC, NDMI, road buffer, NDBI, WRI, SPI, and soil.

It was found that the gravelly loam soil, higher NDBI, elevation ranges between 457 and 904 m, hornblende gneiss rock types, built up areas, moderate slopes, road cuttings, and higher WRI were most strongly associated with landslides in this district. This study found that the FR model has greater prediction capability than the AHP model. According to the FR model, 6.57% area of Idukki district is very highly susceptible to landslides.

The landslide susceptibility maps will be extremely useful to researchers and to the agencies/departments dealing with landslides for implementing suitable mitigation strategies and to develop projects with the objective of landslide risk reduction. The result of this study will help policy makers, planners, and local government to identify the settlements and roads in the high and very high susceptible zones, thereby reducing the risk of landslides in the future.

Declarations

Ethics Approval This article does not contain any studies with human participants or animals performed by any of the authors.

Informed Consent Not applicable.

Conflict of Interest The authors declare no competing interests.

References

Abraham MT, Pothuraju D, Satyam N (2019) Rainfall thresholds for prediction of landslides in Idukki, India: an empirical approach. Water 11(10). https://doi.org/10.3390/w11102113

Abraham MT, Satyam N, Shreyas N, Pradhan B, Segoni S, Maulud KNA, Alamri AM (2021) Forecasting landslides using SIGMA model: a case study from Idukki, India. Geomat Nat Haz Risk 12(1):540–559. https://doi.org/10.1080/19475705.2021.1884610

Achour Y, Boumezbeur A, Hadji R, Chouabbi A, Cavaleiro V, Bendaoud EA (2017) Landslide susceptibility mapping using analytic hierarchy process and information value methods along a highway road section in Constantine, Algeria. Arabian Journal of Geosciences 10(194). https://doi.org/10.1007/s12517-017-2980-6

Achu AL, Joseph S, Aju CD, Mathai J (2021) Preliminary analysis of a catastrophic landslide event on 6 August 2020 at Pettimudi, Kerala State, India. Landslides 18:1459–1463. https://doi.org/10.1007/s10346-020-01598-x

Aghda SMF, Bagheri V, Razifard M (2018) Landslide susceptibility mapping using fuzzy logic system and its influences on mainlines in Lashgarak region, Tehran. Iran Geotechnical and Geological Engineering 36(2):915–937. https://doi.org/10.1007/s10706-017-0365-y

Aimaiti Y, Liu W, Yamazaki F, Maruyama Y (2019) Earthquake-induced landslide mapping for the 2018 Hokkaido Eastern Iburi earthquake using PALSAR-2 data. Remote Sensing 11(20). https://doi.org/10.3390/rs11202351

Ajin RS, Loghin AM, Vinod PG, Jacob MK, Krishnamurthy KK (2016) Landslide susceptible zone mapping using ARS and GIS techniques in selected taluks of Kottayam district, Kerala, India. International Journal of Applied Remote Sensing and GIS 3(1):16–25

Althuwaynee OF, Pradhan B, Park HJ, Lee JH (2014) A novel ensemble bivariate statistical evidential belief function with knowledge-based analytical hierarchy process and multivariate statistical logistic regression for landslide susceptibility mapping. CATENA 114:21–36. https://doi.org/10.1016/j.catena.2013.10.011

Anbalagan R (1992) Landslide hazard evaluation and zonation mapping in mountainous terrain. Eng Geol 32:269–277. https://doi.org/10.1016/0013-7952(92)90053-2

Cancela J, Fico G, Arredondo Waldmeyer MT (2015) Using the analytic hierarchy process (AHP) to understand the most important factors to design and evaluate a telehealth system for Parkinson's disease. BMC Med Inform Decis Mak 15:S7. https://doi.org/10.1186/1472-6947-15-S3-S7

Cardinali M, Galli M, Guzzetti F, Ardizzone F, Reichenbach P, Bartoccini P (2006) Rainfall induced landslides in December 2004 in south-western Umbria, central Italy: types, extent, damage and risk assessment. Nat Hazard 6:237–260

Chawla A, Chawla S, Pasupuleti S, Rao ACS, Sarkar K, Dwivedi R (2018) Landslide susceptibility mapping in Darjeeling Himalayas. Advances in Civil Engineering, India. https://doi.org/10.1155/2018/6416492

Chen W, Han H, Huang B, Huang Q, Fu X (2018) A data-driven approach for landslide susceptibility mapping: a case study of Shennongjia Forestry District. China, Geomatics, Natural Hazards and Risk 9(1):720–736. https://doi.org/10.1080/19475705.2018.1472144

Chen W, Li W, Chai H, Hou E, Li X, Ding X (2016) GIS-based landslide susceptibility mapping using analytical hierarchy process (AHP) and certainty factor (CF) models for the Baozhong region of Baoji city, China. Environmental Earth Sciences 75(63). https://doi.org/10.1007/s12665-015-4795-7

Cruden DM (1991) A simple definition of a landslide. Bull Eng Geol Env 43(1):27–29

Dahoua L, Yakovitch SV, Hadji R, Farid Z (2018) Landslide susceptibility mapping using analytic hierarchy process method in BBA-Bouira Region, case study of East-West Highway, NE Algeria. In: Kallel A, Ksibi M, Ben Dhia H, Khélifi N (eds) Recent advances in environmental science from the Euro-Mediterranean and surrounding regions. EMCEI 2017. Advances in Science, Technology & Innovation (IEREK Interdisciplinary Series for Sustainable Development). Springer, Switzerland: pp 1837–1840. https://doi.org/10.1007/978-3-319-70548-4_532

Dai FC, Lee CF (2002) Landslide characteristics and slope instability modeling using GIS, Lantau Island. Hong Kong Geomorphology 42(3–4):213–228. https://doi.org/10.1016/S0169-555X(01)00087-3

Danumah JH, Odai SN, Saley BM, Szarzynski J, Thiel M, Kwaku A, Kouame FK, Akpa LY (2016) Flood risk assessment and mapping in Abidjan district using multi-criteria analysis (AHP) model and geoinformation techniques, (cote d'ivoire). Geoenvironmental Disasters 3. https://doi.org/10.1186/s40677-016-0044-y

Demir G, Aytekin M, Akgün A, İkizler SB, Tatar O (2013) A comparison of landslide susceptibility mapping of the eastern part of the North Anatolian Fault Zone (Turkey) by likelihood-frequency ratio and analytic hierarchy process methods. Nat Hazards 65:1481–1506. https://doi.org/10.1007/s11069-012-0418-8

Devara M, Tiwari A, Dwivedi R (2021) Landslide susceptibility mapping using MT-InSAR and AHP enabled GIS-based multi-criteria decision analysis. Geomat Nat Haz Risk 12(1):675–693. https://doi.org/10.1080/19475705.2021.1887939

Ehret D, Rohn J, Dumperth C, Eckstein S, Ernstberger S, Otte K, Rudolph R, Wiedenmann J, Xiang W, Bi R (2010) Frequency ratio analysis of mass movements in the Xiangxi catchment, Three Gorges Reservoir area, China. Journal of Earth Science 21:824–834. https://doi.org/10.1007/s12583-010-0134-9

El Jazouli A, Barakat A, Khellouk R (2019) GIS-multicriteria evaluation using AHP for landslide susceptibility mapping in Oum Er Rbia high basin (Morocco). Geoenvironmental Disasters 6(3). https://doi.org/10.1186/s40677-019-0119-7

Elmoulat M, Ait Brahim L (2018) Landslides susceptibility mapping using GIS and weights of evidence model in Tetouan-Ras-Mazari area (Northern Morocco). Geomat Nat Haz Risk 9(1):1306–1325. https://doi.org/10.1080/19475705.2018.1505666

Emrouznejad A, Marra M (2017) The state of the art development of AHP (1979–2017): a literature review with a social network analysis. Int J Prod Res 55(22):6653–6675. https://doi.org/10.1080/00207543.2017.1334976

Gao BC (1996) NDWI—A normalized difference water index for remote sensing of vegetation liquid water from space. Remote Sens Environ 58(3):257–266. https://doi.org/10.1016/S0034-4257(96)00067-3

García-Rodríguez MJ, Malpica JA, Benito B, Díaz M (2008) Susceptibility assessment of earthquake-triggered landslides in El Salvador using logistic regression. Geomorphology 95(3–4):172–191. https://doi.org/10.1016/j.geomorph.2007.06.001

Geertsema M, Highland L, Vaugeouis L (2009) Environmental impact of landslides. In: Sassa K, Canuti P (eds) Landslides – Disaster Risk Reduction. Springer, Berlin, Heidelberg, pp: 589–607. https://doi.org/10.1007/978-3-540-69970-5_31

Guzzetti F, Mondini AC, Cardinali M, Fiorucci F, Santangelo M, Chang KT (2012) Landslide inventory maps: new tools for an old problem. Earth-Science Reviews 112: 42–66. https://doi.org/10.1016/j.earscirev.2012.02.001

Hamza T, Raghuvanshi TK (2017) GIS based landslide hazard evaluation and zonation – a case from Jeldu district, Central Ethiopia. Journal of King Saud University – Science 29(2): 151–165. https://doi.org/10.1016/j.jksus.2016.05.002

Hemasinghe H, Rangali RSS, Deshapriya NL, Samarakoon L (2018) Landslide susceptibility mapping using logistic regression model (a case study in Badulla district, Sri Lanka). Procedia Engineering 212:1046–1053. https://doi.org/10.1016/j.proeng.2018.01.135

Hong Y, Adler RF, Huffman GJ (2007) Satellite remote sensing for global landslide monitoring. EOS Trans Am Geophys Union 88(37):357–368

Huang F, Yao C, Liu W, Li Y, Liu X (2018) Landslide susceptibility assessment in the Nantian area of China: a comparison of frequency ratio model and support vector machine. Geomat Nat Haz Risk 9(1):919–938. https://doi.org/10.1080/19475705.2018.1482963

Ibrahim GRF (2017) Urban land use land cover changes and their effect on land surface temperature: case study using Dohuk City in the Kurdistan Region of Iraq. Climate 5(1). https://doi.org/10.3390/cli5010013

Jaafari A, Najafi A, Pourghasemi HR, Rezaeian J, Sattarian A (2014) GIS-based frequency ratio and index of entropy models for landslide susceptibility assessment in the Caspian forest, northern Iran. Int J Environ Sci Technol 11(4):909–926. https://doi.org/10.1007/s13762-013-0464-0

Kanungo DP, Arora MK, Sarkar S, Gupta RP (2006) A comparative study of conventional, ANN black box, fuzzy and combined neural and fuzzy weighting procedures for landslide susceptibility zonation in Darjeeling Himalayas. Eng Geol 85(3–4):347–366. https://doi.org/10.1016/j.enggeo.2006.03.004

Kanungo DP, Arora MK, Sarkar S, Gupta RP (2009) Landslide susceptibility zonation (LSZ) mapping - a review. Journal of South Asia Disaster Studies 2(1):81–105

Kanungo DP, Singh R, Dash RK (2020) Field observations and lessons learnt from the 2018 landslide disasters in Idukki district, Kerala. India Current Science 119(11):1797–1806

Karsli F, Atasoy M, Yalcin A, Reis S, Demir O, Gokceoglu C (2009) Effects of land-use changes on landslides in a landslide-prone area (Ardesen, Rize, NE Turkey). Environ Monit Assess 156:241–255. https://doi.org/10.1007/s10661-008-0481-5

Kaur H, Gupta S, Parkash S (2017) Comparative evaluation of various approaches for landslide hazard zoning: a critical review in Indian perspectives. Spat Inf Res 25(3):389–398. https://doi.org/10.1007/s41324-017-0105-7

Kayastha P, Dhital MR, De Smedt F (2012) Landslide susceptibility mapping using the weight of evidence method in the Tinau watershed. Nepal Natural Hazards 63(2):479–498. https://doi.org/10.1007/s11069-012-0163-z

Khan H, Shafique M, Khan MA, Bacha MA, Shah SU, Calligaris C (2019) Landslide susceptibility assessment using frequency ratio, a case study of northern Pakistan. The Egyptian Journal of Remote Sensing and Space Science 22(1):11–24. https://doi.org/10.1016/j.ejrs.2018.03.004

Kouhpeima A, Feiznia S, Ahmadi H, Moghadamnia AR (2017) Landslide susceptibility mapping using logistic regression analysis in Latyan catchment. Desert 22(1): 85–95. https://doi.org/10.22059/jdesert.2017.62181

Kumar R, Anbalagan R (2016) Landslide susceptibility mapping using analytical hierarchy process (AHP) in Tehri reservoir rim region, Uttarakhand. J Geol Soc India 87(3):271–286. https://doi.org/10.1007/s12594-016-0395-8

Kumar MK, Annadurai R (2015) Comparison of frequency ratio model and analytic hierarchy process methods upon landslide susceptibility mapping using geospatial techniques. Disaster Advances 8(5):46–55

Kumar D, Thakur M, Dubey CS, Shukla DP (2017) Landslide susceptibility mapping & prediction using support vector machine for Mandakini river basin, Garhwal Himalaya, India. Geomorphology 295:115–125. https://doi.org/10.1016/j.geomorph.2017.06.013

Lee S (2007) Landslide susceptibility mapping using an artificial neural network in the Gangneung area. Korea International Journal of Remote Sensing 28(21):4763–4783. https://doi.org/10.1080/01431160701264227

Lee S, Pradhan B (2006) Probabilistic landslide hazards and risk mapping on Penang Island, Malaysia. J Earth Syst Sci 115:661–672. https://doi.org/10.1007/s12040-006-0004-0

Lee S, Talib JA (2005) Probabilistic landslide susceptibility and factor effect analysis. Environmental Geology 47:982–990. https://doi.org/10.1007/s00254-005-1228-z

Lee S, Choi J, Min K (2004) Probabilistic landslide hazard mapping using GIS and remote sensing data at Boun. Korea International Journal of Remote Sensing 25(11):2037–2052. https://doi.org/10.1080/01431160310001618734

Lee ML, Ng KY, Huang YF, Li WC (2014) Rainfall-induced landslides in Hulu Kelang area. Malaysia Natural Hazards 70(1):353–375. https://doi.org/10.1007/s11069-013-0814-8

Li F, He H (2018) Assessing the accuracy of diagnostic tests. Shanghai Archives of Psychiatry 30(3): 207–212. https://doi.org/10.11919/j.issn.1002-0829.218052

Melo F (2013) Area under the ROC curve. In: Dubitzky W, Wolkenhauer O, Cho KH, Yokota H (eds) Encyclopedia of Systems Biology. Springer, New York. https://doi.org/10.1007/978-1-4419-9863-7_209

Moore ID, Grayson RB, Ladson AR (1991) Digital terrain modelling: a review of hydrological, geomorphological, and biological applications. Hydrol Process 5(1):3–30. https://doi.org/10.1002/hyp.3360050103

Myronidis D, Papageorgiou C, Theophanous S (2016) Landslide susceptibility mapping based on landslide history and analytic hierarchy process (AHP). Nat Hazards 81(1):245–263. https://doi.org/10.1007/s11069-015-2075-1

Nakamura S, Wakai A, Umemura J, Sugimoto H, Takeshi T (2014) Earthquake-induced landslides: distribution, motion and mechanisms. Soils Found 54(4):544–559. https://doi.org/10.1016/j.sandf.2014.06.001

Nakileza BR, Nedala S (2020) Topographic influence on landslides characteristics and implication for risk management in upper Manafwa catchment, Mt Elgon Uganda. Geoenvironmental Disasters 7.https://doi.org/10.1186/s40677-020-00160-0

Oh HJ, Pradhan B (2011) Application of a neuro-fuzzy model to landslide-susceptibility mapping for shallow landslides in a tropical hilly area. Comput Geosci 37(9):1264–1276. https://doi.org/10.1016/j.cageo.2010.10.012

Oh HJ, Lee S, Hong SM (2017) Landslide susceptibility assessment using frequency ratio technique with iterative random sampling. Journal of Sensors. https://doi.org/10.1155/2017/3730913

Oh HJ, Kadavi PR, Lee CW, Lee S (2018) Evaluation of landslide susceptibility mapping by evidential belief function, logistic regression and support vector machine models. Geomat Nat Haz Risk 9(1):1053–1070. https://doi.org/10.1080/19475705.2018.1481147

Ortiz JAV, Martínez-Graña AM (2018) A neural network model applied to landslide susceptibility analysis (Capitanejo, Colombia). Geomat Nat Haz Risk 9(1):1106–1128. https://doi.org/10.1080/19475705.2018.1513083

Park SJ, Lee CW, Lee S, Lee MJ (2018) Landslide susceptibility mapping and comparison using decision tree models: a case study of Jumunjin area, Korea. Remote Sens 10.https://doi.org/10.3390/rs10101545

Pham VD, Nguyen Q, Nguyen H, Pham V, Vu VM, Bui Q (2020) Convolutional neural network—optimized moth flame algorithm for shallow landslide susceptible analysis. IEEE Access 8:32727–32736. https://doi.org/10.1109/ACCESS.2020.2973415

Pourghasemi HR, Mohammady M, Pradhan B (2012a) Landslide susceptibility mapping using index of entropy and conditional

probability models in GIS: Safarood Basin. Iran CATENA 97:71–84. https://doi.org/10.1016/j.catena.2012.05.005

Pourghasemi HR, Pradhan B, Gokceoglu C (2012b) Application of fuzzy logic and analytical hierarchy process (AHP) to landslide susceptibility mapping at Haraz watershed. Iran Natural Hazards 63(2):965–996. https://doi.org/10.1007/s11069-012-0217-2

Pourghasemi HR, Jirandeh AG, Pradhan B, Xu C, Gokceoglu C (2013) Landslide susceptibility mapping using support vector machine and GIS at the Golestan Province. Iran Journal of Earth System Science 122(2):349–369

Pradhan B, Lee S (2010) Landslide susceptibility assessment and factor effect analysis: backpropagation artificial neural networks and their comparison with frequency ratio and bivariate logistic regression modelling. Environ Model Softw 25(6):747–759. https://doi.org/10.1016/j.envsoft.2009.10.016

Pradhan B, Sezer EA, Gokceoglu C, Buchroithner MF (2010) Landslide susceptibility mapping by neuro-fuzzy approach in a landslide-prone area (Cameron Highlands, Malaysia). IEEE Trans Geosci Remote Sens 48(12):4164–4177. https://doi.org/10.1109/TGRS.2010.2050328

Raghuvanshi TK, Ibrahim J, Ayalew D (2014) Slope stability susceptibility evaluation parameter (SSEP) rating scheme-an approach for landslide hazard zonation. J Afr Earth Sc 99(2):595–612. https://doi.org/10.1016/j.jafrearsci.2014.05.004

Raghuvanshi TK, Negassa L, Kala PM (2015) GIS based grid overlay method versus modeling approach – a comparative study for landslide hazard zonation (LHZ) in Meta Robi district of West Showa Zone in Ethiopia. The Egyptian Journal of Remote Sensing and Space Sciences 18:235–250. https://doi.org/10.1016/j.ejrs.2015.08.001

Ramachandran RM, Reddy CS (2017) Monitoring of deforestation and land use changes (1925–2012) in Idukki district, Kerala, India using remote sensing and GIS. Journal of the Indian Society of Remote Sensing 45:163–170. https://doi.org/10.1007/s12524-015-0521-x

Rasyid AR, Bhandary NP, Yatabe R (2016) Performance of frequency ratio and logistic regression model in creating GIS based landslides susceptibility map at Lompobattang Mountain, Indonesia. Geoenvironmental Disasters 3.https://doi.org/10.1186/s40677-016-0053-x

Ray RL, Jacobs JM (2007) Relationships among remotely sensed soil moisture, precipitation and landslide events. Nat Hazards 43:211–222. https://doi.org/10.1007/s11069-006-9095-9

Resmi TR, Sudharma KV, Hameed AS (2016) Stable isotope characteristics of precipitation of Pamba river basin, Kerala, India. J Earth Syst Sci 125:1481–1493. https://doi.org/10.1007/s12040-016-0747-1

Rostami ZA, Al-modaresi SA, Fathizad H, Faramarzi M (2016) Landslide susceptibility mapping by using fuzzy logic: a case study of Cham-gardalan catchment, Ilam, Iran. Arabian Journal of Geosciences 9(685). https://doi.org/10.1007/s12517-016-2720-3

Roy J, Saha S (2019) Landslide susceptibility mapping using knowledge driven statistical models in Darjeeling District, West Bengal, India. Geoenvironmental Disasters 6.https://doi.org/10.1186/s40677-019-0126-8

Russo RFSM, Camanho R (2015) Criteria in AHP: a systematic review of literature. Procedia Computer Science 55:1123–1132. https://doi.org/10.1016/j.procs.2015.07.081

Saaty TL (1980) The analytic hierarchy process: planning, priority setting, resource allocation (decision making series). McGraw Hill, New York, United States of America

Sar N, Chatterjee S, Adhikari MD (2015) Integrated remote sensing and GIS based spatial modelling through analytical hierarchy process (AHP) for water logging hazard, vulnerability and risk assessment in Keleghai river basin, India. Model Earth Syst Environ 1.https://doi.org/10.1007/s40808-015-0039-9

Sarkar S, Kanungo DP, Mehrotra GS (1995) Landslide hazard zonation: a case study of Gharwal Himalaya. India Mountain Research and Development 15(4):301–309

Sartohadi J, Pulungan NAHJ, Nurudin M, Wahyudi W (2018) The ecological perspective of landslides at soils with high clay content in the Middle Bogowonto Watershed, Central Java, Indonesia. Applied and Environmental Soil Science. https://doi.org/10.1155/2018/2648185

Sassa K, Fukuoka H, Scarascia-Mugnozza G, Evans S (1996) Earthquake-induced-landslides: distribution, motion and mechanisms. Soils Found 36:53–64. https://doi.org/10.3208/sandf.36.Special_53

Semlali I, Ouadif L, Bahi L (2019) Landslide susceptibility mapping using the analytical hierarchy process and GIS. Curr Sci 116(5):773–779

Senthilkumar V, Chandrasekaran SS, Maji VB (2018) Rainfall-induced landslides: case study of the Marappalam landslide, Nilgiris district, Tamil Nadu, India. International Journal of Geomechanics 18(9). https://doi.org/10.1061/(ASCE)GM.1943-5622.0001218

Shahfahad, Kumari B, Tayyab M, Ahmed IA, Baig MRI, Khan MF, Rahman (2020) A longitudinal study of land surface temperature (LST) using mono- and split-window algorithms and its relationship with NDVI and NDBI over selected metro cities of India. Arab J Geosci 13.https://doi.org/10.1007/s12517-020-06068-1

Shahri AA, Spross J, Johansson F, Larsson S (2019) Landslide susceptibility hazard map in southwest Sweden using artificial neural network. CATENA 183.https://doi.org/10.1016/j.catena.2019.104225

Shano L, Raghuvanshi TK, Meten M (2021) Landslide susceptibility mapping using frequency ratio model: the case of Gamo highland, South Ethiopia. Arab J Geosci 14.https://doi.org/10.1007/s12517-021-06995-7

Sharma S, Mahajan AK (2018) Comparative evaluation of GIS-based landslide susceptibility mapping using statistical and heuristic approach for Dharamshala region of Kangra Valley, India. Geoenvironmental Disasters 5(4). https://doi.org/10.1186/s40677-018-0097-1

Shen L, Li C (2010) Water body extraction from Landsat ETM+ imagery using adaboost algorithm. 2010 18th International Conference on Geoinformatics: 1–4. https://doi.org/10.1109/GEOINFORMATICS.2010.5567762

Sifa SF, Mahmud T, Tarin MA, Haque DME (2019) Event-based landslide susceptibility mapping using weights of evidence (WoE) and modified frequency ratio (MFR) model: a case study of Rangamati district in Bangladesh. Geology, Ecology, and Landscapes. https://doi.org/10.1080/24749508.2019.1619222

Silalahi FES, Pamela, Arifianti Y, Hidayat F (2019) Landslide susceptibility assessment using frequency ratio model in Bogor, West Java, Indonesia. Geosci Lett 6.https://doi.org/10.1186/s40562-019-0140-4

Sujatha ER, Sridhar V (2021) Landslide susceptibility analysis: a logistic regression model case study in Coonoor, India. Hydrology 8(1). https://doi.org/10.3390/hydrology8010041

Turrini MC, Visintainer P (1998) Proposal of a method to define areas of landslide hazard and application to an area of the Dolomites. Italy Engineering Geology 50(3–4):255–265. https://doi.org/10.1016/S0013-7952(98)00022-2

United States Geological Survey (2004) Landslide types and processes. Fact Sheet 2004–3072. U.S. Department of the Interior.

Wu Y, Li W, Liu P, Bai H, Wang Q, He J, Liu Y, Sun S (2016) Application of analytic hierarchy process model for landslide

susceptibility mapping in the Gangu County, Gansu Province, China. Environmental Earth Sciences 75(422). https://doi.org/10.1007/s12665-015-5194-9

Xie P, Wen H, Ma C, Baise LG, Zhang J (2018) Application and comparison of logistic regression model and neural network model in earthquake-induced landslides susceptibility mapping at mountainous region, China. Geomat Nat Haz Risk 9(1):501–523. https://doi.org/10.1080/19475705.2018.1451399

Zha Y, Gao J, Ni S (2003) Use of normalized difference built-up index in automatically mapping urban areas from TM imagery. Int J Remote Sens 24(3):583–594. https://doi.org/10.1080/01431160304987

Zhang K, Thapa B, Ross M, Gann D (2016) Remote sensing of seasonal changes and disturbances in mangrove forest: a case study from South Florida. Ecosphere 7(6). https://doi.org/10.1002/ecs2.1366

Zhang K, Wu X, Niu R, Yang K, Zhao L (2017) The assessment of landslide susceptibility mapping using random forest and decision tree methods in the Three Gorges Reservoir area, China. Environ Earth Sci 76.https://doi.org/10.1007/s12665-017-6731-5